Methanol synthesis via CO_2 hydrogenation: Analysis and simulation of kinetic performance using typical industrial conditions

by

J Garrett Alexander

B.S., University of Houston – Clear Lake, 2010
M.S., University of Houston, 2017

A REPORT

submitted in partial fulfillment of the requirements for the degree

MASTER OF SCIENCE

Department of Chemical Engineering
Carl R. Ice College of Engineering

KANSAS STATE UNIVERSITY
Manhattan, Kansas

2021

Approved by:

Major Professor
Dr. Placidus Amama

Abstract

Due to the substantial increase in anthropogenic carbon dioxide (CO_2) emissions over the past century, multiple technologies are being explored to capture this greenhouse gas and utilize it as a viable feedstock. A promising outlet for CO_2 is hydrogenation to methanol. Methanol is widely used in the chemical industry, primarily in the production of formaldehyde, methyl-tert-butyl-ether, and acetic acid, as well as an alternative to traditional fuels due to its superior combustion properties. In addition, significant research is ongoing to utilize methanol as an energy carrier for use in fuel cells. Significant research has been done to understand the kinetic performance of $Cu/ZnO/Al_2O_3$ catalyst for methanol synthesis, however, much of this research involves lower pressures (<55 bar) than is used in many industrial methanol synthesis processes (80-120 bar). In addition, the H_2 to CO_2 ratio in the reactor feed that is used in industry is significantly higher than what was used to develop many of the kinetic experiments and associated models found in the literature review.

This work explores the development of a methanol synthesis catalyst including a thorough literature review of catalyst properties, deactivation, and kinetic mechanisms. The catalytic performance of $Cu/ZnO/Al_2O_3$ catalyst was explored using a kinetic model developed in MATLAB. The results highlight the negative effect that CO in the feed has on conversion at high H_2 to CO_2 ratios. Pressure drop across a packed bed reactor using typical industrial conditions was also simulated and determined to be negligible for typical reactor configurations and catalyst properties. The effects of non-ideality on reactor performance were simulated using industrial methanol synthesis conditions. The results show up to a 5 percent increase in CO_2 conversion is predicted when including thermodynamic effects in the reactor simulation. This phenomenon can be explained by the reduction of partial pressure of the products formed via the methanol synthesis reaction and therefore a shift in equilibrium towards methanol production.

Table of Contents

List of Figures

List of Tables

List of Symbols and Terms

f_i	fugacity of component *i* (bar)
$\Delta G^0(T)$	standard change in Gibbs free energy as a function of T (J)
$\Delta H^0(T)$	standard change in enthalpy as a function T (J)
H.s	hydrogen attached to active site
K^*_{redox}	equilibrium constant for redox mechanism
K^*_1	equilibrium constant for (R1)
K^*_2	equilibrium constant for (R2)
K^*_3	equilibrium constant for (R3)
K_{CO}	adsorption equilibrium constant for CO (bar^{-1})
K_{CO_2}	adsorption equilibrium constant for CO_2 (bar^{-1})
K_{H_2O}	adsorption equilibrium constant for H_2O (bar^{-1})
O.s	oxygen attached to active site
P	pressure (bar)
P_c	critical pressure (bar)
p_i	partial pressure of component *i* (bar)
r_i	reaction rate per weight of catalyst for (R_i) (mol s^{-1} kg^{-1})
R	gas constant (J K^{-1} mol^{-1})
s	active site
T	temperature (K)
T_c	critical temperature (K)
T_{ref}	reference temperature (K)
y_i	mole fraction of component *i* (unitless)

φ_i^V	fugacity coefficient of component i
ω	acentric factor (unitless)

Chapter 1 - Literature Review

1.1 Introduction

The concentration of carbon dioxide (CO_2) in the atmosphere has increased substantially since the dawn of the industrial age in the nineteenth century [1]. According to the International Energy Agency (IEA), CO_2 emissions from the energy sector will increase 43% by 2035, therefore substantial efforts are underway to reduce CO_2 emissions, including developing alternative ways to capture and utilize the carbon source as a valuable feedstock [2]. CO_2 is produced naturally by all aerobic organisms when they metabolize organic compounds to produce energy by respiration, during the decay of organic materials, and by the combustion of carbon-containing fuels.

CO_2 is an important compound utilized in many commercial applications in the food, oil, and chemical industry. It is commonly used as an inert gas in industrial applications such as welding and fire extinguishers, but also as a feedstock used to produce many common chemicals. Globally, approximately 230 million tonnes (Mt) of CO_2 are used every year [3]. The largest consumer is the fertilizer industry, where 130 Mt CO_2 is used in urea manufacturing, followed by oil and gas, with a consumption of 70 to 80 Mt CO_2 for enhanced oil recovery [4]. An emerging market is CO_2 based fuels, but these are generally energy intensive to produce and require significant amounts of hydrogen so exploring ways to reduce manufacturing costs through innovative technology is imperative for CO_2 fuels to be able to compete with traditional petroleum fuels.

A primary use of CO_2 in the chemical industry is in methanol production. Methanol is an important precursor to many commodity chemicals including formaldehyde, acetic acid, methyl-tert-butyl-ether, as well as an alternative fuel to gasoline. Methanol has been identified as a promising energy carrier because it is easier to store than hydrogen and natural gas, although its energy density is somewhat lower than ethanol and gasoline [4]. Additional advantages of methanol include its biodegradability and water solubility. The half-life for methanol in groundwater is one to seven days while many gasoline components can be as high as hundreds of

days. Methanol's high water solubility reduces the risk of high concentrations accumulating in ground and surface water supplies as well as most natural habitats [5].

As of 2020, an estimated 90 million metric tons of methanol is produced per year with natural gas as the principal feedstock [6]. Natural gas is typically converted to syngas via the endothermic process called reforming where CO, CO_2, and H_2 are generated as the products. This process requires high temperatures, and therefore significant quantities of CO_2 are emitted from the reforming furnaces, thus negating the net CO_2 reduction from the conversion of the CO_2 feedstock. Ongoing research is focused on developing competitive technologies to "capture" the CO_2 emitted from these types of industrial processes for use as a viable feedstock [7].

Emerging technologies such as CO_2 capture offer promising solutions to help mitigate the climate change crisis. However, significant work must still be done to make these costs competitive with traditional processes on an industrial scale. The objective of this paper is to provide a thorough analysis of methanol synthesis reaction technology with a focus on providing a better understanding of the kinetic mechanisms provided in previous work and demonstrate its use through a rigorous one-dimensional model incorporating typical industrial operating conditions. This improved understanding is critical to overcoming the monumental challenge of transforming emerging CO_2 reduction technologies to cost competitive solutions that compete with traditional processes.

1.2 Catalyst History

Methanol was initially produced by the pyrolysis of wood, which is why methanol is sometime referred to as "wood alcohol" [8]. The wood was heated, which released methanol gas as it slowly burned. The gas was then collected and condensed to produce liquid methanol. Given the relatively slow process, producing only ~6 gallons of methanol per ton of wood, and the intense energy demand, there became a growing interest in discovering alternate routes to produce methanol [9].

Methanol synthesis by hydrogenation of carbon monoxide was proposed by Paul Sabatier in 1905, a French chemist. BASF later commercialized this approach during World War II at their manufacturing plant in Leuna, Germany. BASF developed a means to convert synthesis gas into methanol. The process used a heterogenous catalyst composed of zinc chromite catalyst to provide a kinetic advantage over the thermodynamically favored production of aliphatic hydrocarbons. The reaction kinetics for this catalyst were relatively slow, so the process had to be operated at temperatures up to 400ºC and 300 bar to reach an acceptable production rate [10].

Early in the 1960s, Imperial Chemical Industries (ICI) developed the Low Pressure Methanol process (LPM) which was significantly more efficient than the high pressure process used at that time. This process introduced the use of ternary catalysts containing copper, zinc, and chromium. This catalyst enabled relatively fast reaction rates at low pressure (30-120 bar) and lower reactor temperatures (200-300ºC), as well as high selectivity (~99.5%). Shortly after the initial application was filed in 1963, another patent application was filed by ICI that included the use of oxides of copper and zinc, was well aluminum [10]. Most catalysts used today in industrial scale methanol production utilize some combination of these compounds [11].

1.3 Role of Promoter

The Cu sites are believed to be the only active sites, however, ZnO is added as a promotor that significantly increases the catalyst activity [12]. Several theories have been suggested as to the role that ZnO plays in this process. These include gas-dependent morphological changes of Cu on ZnO, support induced strain, and strong metal-support interaction (SMSI) [13]. Recent studies have shown that the active sites are correlated with step sites on the metal surface and perhaps the migration of Zn atoms into these sites. This proposed behavior aligns with experimental observations that have shown fully or partially reduced Zn atoms in the Cu surface after reduction of the $Cu/ZnO/Al_2O_3$ catalyst.

A recent study conducted by the Center for Individual Nanoparticle Functionality (CINF) attempted to improve the characterization of the catalyst properties and develop correlations

aimed at improving the catalytic efficiency [13]. The study utilized multiple characterization techniques such as surface area titration, electron microscopy, activity measurement, density functional theory calculations, and modeling of the catalyst before and after catalyst reduction and after methanol synthesis.

The results of the study suggest the primary species attached to the Cu particle surface in $Cu/ZnO/Al_2O_3$ catalyst is a Cu-Zn surface alloy instead of a ZnOx layer as previously reported by similar studies [13]. It has been theorized that the formate species, which is thought to be the most abundant intermediate produced in the reaction, absorbed on the catalyst surface during the synthesis process, may affect catalyst activity. This study found, however, that the concentration of the format species is so low, with the high coverage of formate at the few step sites and low coverage at the abundant terrace sites under typical methanol synthesis conditions, that the catalyst activity should be unaffected. It was also concluded that the Zn atoms may be partially oxidized during the synthesis process given the attachment of formate and other oxygen containing species, which explains the analytical results showing the presence of Zn atoms in the formate complex, but the primary form of Zn is in the reduced state.

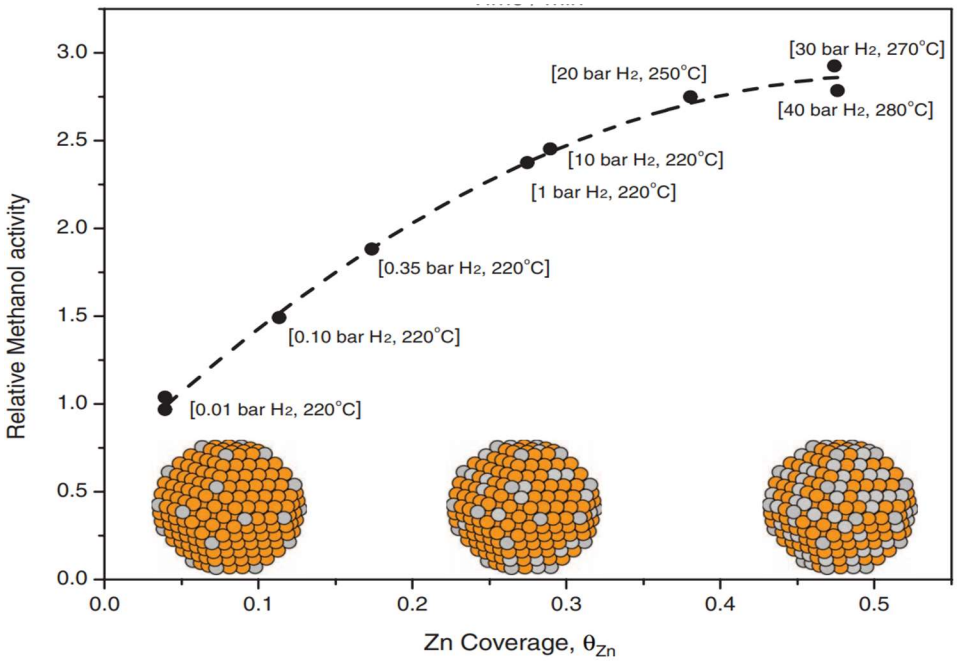

Figure 1-1: Catalyst activity as a function of Zn coverage [13].

Another surprising finding from the CINF study was the correlation of Cu and Zn particle sizes with catalyst activity. The tendency is to believe the catalyst activity would increase as the particle size of the active component, in this case Cu, decreases as the surface area increases thus allowing more active sites for the gas molecules. This study, however, predicts the opposite is true. Figure 1-3 shows that the catalyst activity decreases as the Cu particles decrease. In fact, as shown by Figure 1-2, this work predicts the catalyst activity will increase as the promoter atoms (Zn) increase. It is believed that this phenomenon can be explained by the thermodynamic mechanism of the Zn-Cu interaction, and the subsequent migration of reduced Zn particles that directly influence the catalyst activity. It is noted, however, this mechanism was only hypothesized via modeling and was not observed experimentally.

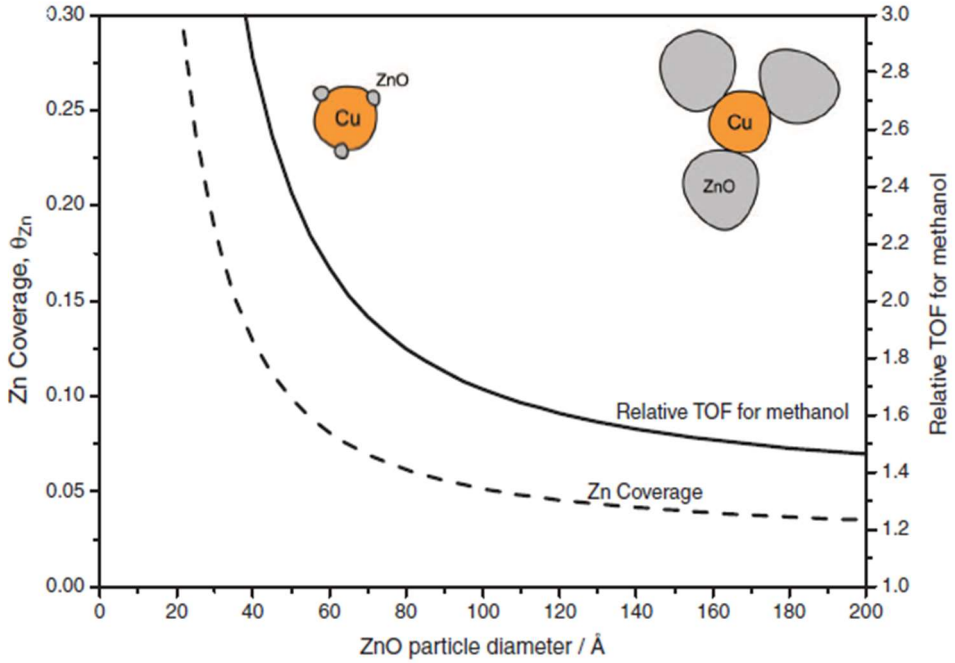

Figure 1-2: Catalyst efficiency as a function of Zn coverage and ZnO particle size [13].

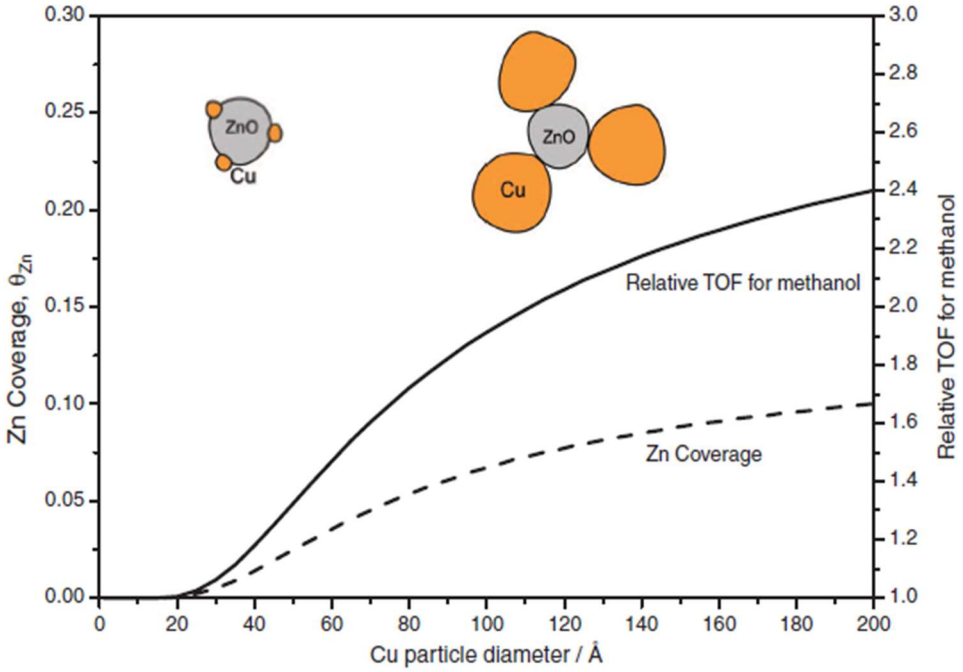

Figure 1-3: Catalyst efficiency as a function of Zn coverage and Cu particle size [13].

1.4 Role of Support

The role that catalyst support plays in catalyst activity has also been investigated. Alumina, Al_2O_3, is added as a support material to increase the thermal stability and surface exposure of active sites to the reaction [12]. The specific surface area of the catalyst has been shown to increase with the ratio of Al to Cu/ZnO and therefore a potential increase in the active metal surface area as well. One would believe an increase in active metal surface area would lead to an increase in catalyst activity, but this is not always the case. Studies have shown that the intrinsic activity of Cu is influenced by the specific surface area and that an optimal catalyst activity is achieved between 85 m^2/g and 115 m^2/g. This suggests that alumina may directly influence the active sites beyond its function as a support. The alumina also provides thermal stability to the catalyst. After successive thermal treatment at 400°C, the catalyst tends to lose activity with a decreasing ratio of support material. The optimal ratio of support to Cu is between 10:1 to 12:1, as depicted in Figure 1-4.

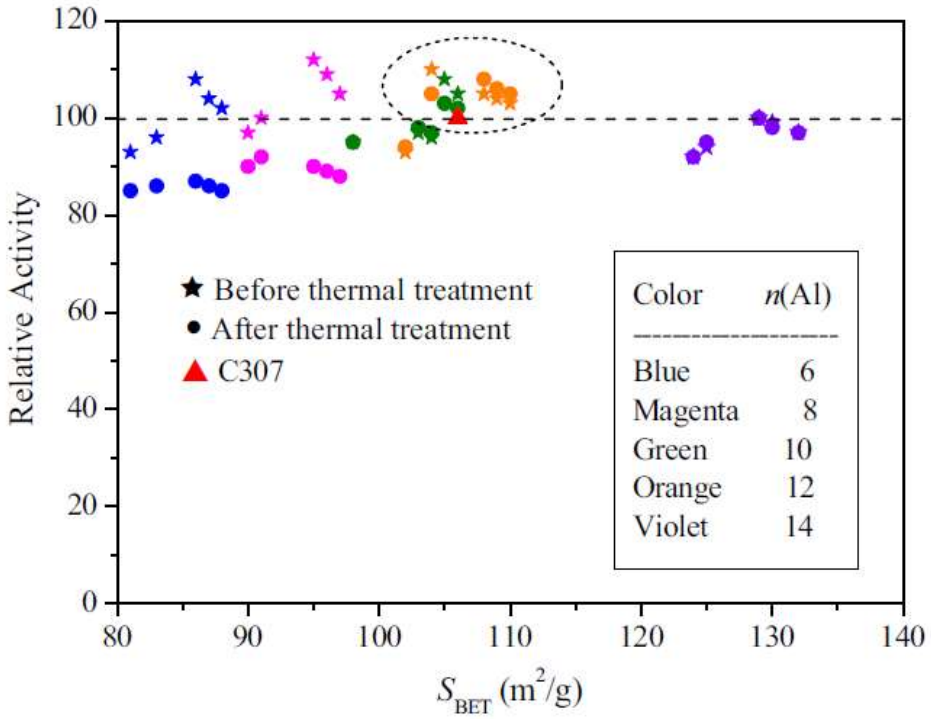

Figure 1-4: Catalyst activity as a function of specific surface area (S_{BET}) [12].

1.5 Other Emerging Catalyst

Various types of supported precious metals have been investigated for use in methanol synthesis. Fujitani et al. [14] first reported the use of Pd-based catalyst using Ga_2O_3 support which was shown to increase the methanol yield by a factor of two and the turnover frequency by a factor of 20 over that of $Cu/ZnO/Al_2O_3$. This improvement was theorized to be from new metallic catalytic functions formed by Pd-Ga alloy formed on the surface. Another study found that small amounts of Ga_2O_3 added to Pd/SiO_2 produced an equally dramatic enhancement of the catalyst performance for the generation of oxygenated compounds, and therefore its application in methanol synthesis was also explored. The mechanisms responsible for the improved performance were found to be substantially different. Structural analysis of the Ga_2O_3-Pd/SiO_2 complex showed there was no Pd-Ga alloy present on the catalyst surface. It was found that dissociated hydrogen was generated by Pd^0 away from the Ga_2O_3 support and then migrated over to reach the reactive formate species to complete the reaction cycle, a process known as hydrogen spillover [15] .

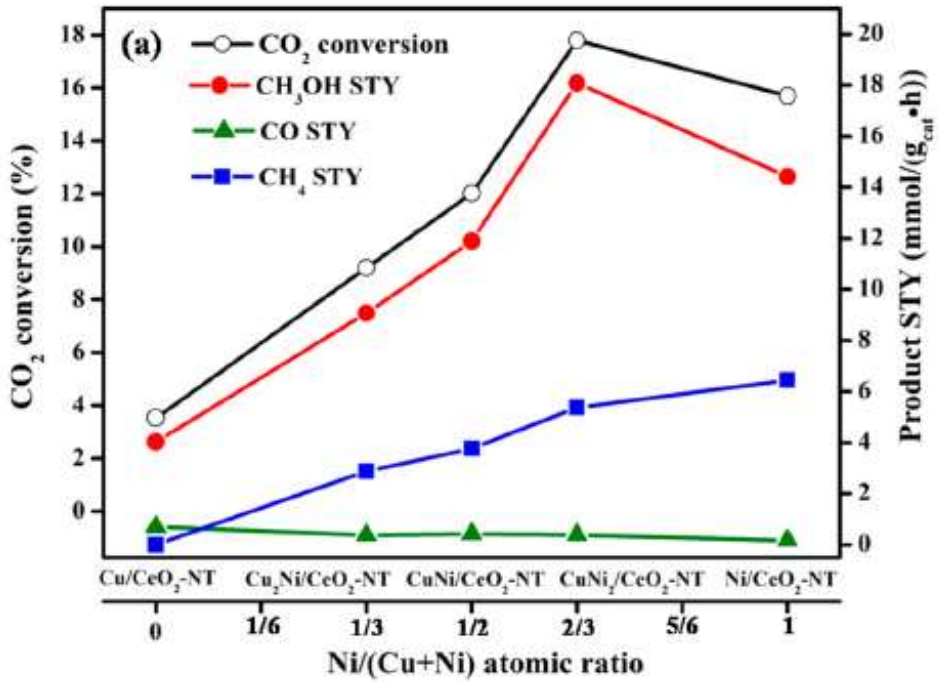

Figure 1-5: Cu-Ni/CeO_2 catalyst performance as a function of Ni concentration [16]**.**

Additional bimetallic catalysts have been explored for methanol synthesis. Work done by Tan et al. [16] investigated the use of Cu-Ni/CeO_2 nanotubes for CO_2 hydrogenation to methanol. The results show a remarkable improvement in the selectivity and STY over that of the traditional Cu/ZnO/Al_2O_3 catalyst. A synergistic effect between Ni and Cu was observed that improves the dispersion and reducibility of the bimetallic Cu-Ni system but also reduces the activation energy as well as promotes CO adsorption and hydrogenation to methanol. Furthermore, the partial reduction of Ce^{4+} to Ce^{3+} induced by the strong Cu-Ni interaction excites the electronic properties of the surface oxygen and results in excess oxygen vacancies to adsorb and activate CO_2 [2]. Figure 1-5 shows the catalytic performance of Cu-Ni/CeO_2 nanotube catalyst as a function of Ni content on the catalyst surface.

With the recent developments in the use of carbon nanotubes (CNTs) for catalyst support, several recent studies have investigated the use of CNTs in methanol syntheses due to their high surface area and thermal conductivity. Multiwalled CNTs (MWCNTs) have been explored as a possible support material or promoter for methanol synthesis catalyst. Two predominate types of MWCNT have been developed, a concentric and herringbone type [17]. A concentric MWCNT (c-MWCNT) has coaxially arranged single walled CNTs with regularly increasing diameters. The inner tube distance is typically the same as the intergraphene distance in polyaromatic solids (0.34 nm). Each atom faces either a ring center or a carbon atom in the neighboring plane, which allows for nanotube cores that are wrapped over one another and thus minimizing the free energy for larger tubes to exist. These nanotube cores eventually become wrapped by multiwall structures resembling graphene sheets at high temperatures. Herringbone MWCTs (h-MWCNT) are generated by the catalyst-enhanced thermal cracking of hydrocarbons and exhibit various graphene angles within the nanotube walls that look like pinched walls inside or outside of the tubes. The nanotubes stack on one other creating a bamboo-like structure [18].

A recent study by Kong et al. [17] demonstrated an ~40 percent improvement in methanol yield by the use of CNT versus Ga_2O_3 support alone. The study concluded that the addition of CNT did not cause a noticeable change in the activation energy of the CO_2 hydrogenation reaction, but rather it increased the molar percentage of the catalytically active Pd^0 species in the total amount of Pd at the surface of the catalyst. This improved the capability

of the catalyst to adsorb and activate additional H_2 to proceed in the reaction process. The type of CNT also played a significant role in the promotion effect of the CNT support. The use of c-MWNT was shown to possess a less active surface with less dangling bonds over the h-type and therefore had a lower capacity for adsorbing H_2 [17].

A list of the various catalyst materials explored in this work is presented in Table 1-1. Although $Cu/ZnO/Al_2O_3$ remains the dominate catalyst used in industry, other noble materials such as CNTs and bimetallic alloys provide potential improvements in methanol synthesis technology. Additional work needs to be done to quantify the economic benefits and feasibility of utilizing these materials on an industrial scale.

Table 1-1 – Performance of methanol synthesis catalyst explored in literature review.

Catalyst Description	Support Material	X (CO-hydro.)(%)	X (CO2-hydro.) (%)	Selectivity of CH_3OH (C%)	STY of CO2 to CH_3OH (mg/(h*g))	T (K)	P (Mpa)
$16\%Pd_{0.1}Zn_1$/CNTs(h-type)	CNTs		6.3	99.6	37	523	3.0
$22\%Pd_{0.1}Zn_1$/CNTs(p-type)	CNTs		6.2	95.2	35	523	3.0
$35\%Pd_{0.1}Zn_1$/AC	AC		4.9	96.5	28	523	3.0
$20\%Pd_{0.1}Zn_1/\gamma\text{-}Al_2O_3$	Al_2O_3		4.4	92.1	24	523	3.0
Commercial	Al_2O_3	40.8	16.3		151	513	4.0
Cu:Zn:Al:Zr (mole ratio 6:3:0.5:0.5) without CNT	Al_2O_3	50.9	20.5		261	513	4.0
Cu:Zn:Al:Zr (mole ratio 6:3:0.5:0.5) with CNT	CNTs	54.5	21.5		282	513	4.0
Cu-Ni/SiO_2	SiO_2	12.1		99.0	167	548	10.0
Cu-Ni/γ-Al_2O_3	Al_2O_3	27.0		27.2	189	563	2.0
Cu-Pd/CeO_2	CeO_2		16.1	26.7	29	543	3.0
$Cu/ZnO/Al_2O_3$	Al_2O_3		23.1	31.2	311	533	3.0
$CuNi_2/CeO_2$-NT	CeO_2-NT		17.8	78.8	580	533	3.0
Pd_1Ga_{10}-12.6%(3%Pd/CNTs(h-type))	CNTs		9.8	95.7	555	523	5.0
Pd_1Ga_{10}-12.6%CNTs(h-type)	CNTs		9.0	96.2	512	523	5.0
Pd_1Ga_{10}	Ga_2O_3		8.6	94.5	480	523	5.0
Pd_1Ga_{10}-12.6%CNTs(p-type)	CNTs		7.5	96.6	428	523	5.0
3%Pd/CNTs(h-type)	CNTs		3.6	0	0	523	5.0
$Pd_{0.1}Zin_1$-10%(5.0 %Pd/CNTs)	CNTs		7.0	99.8	343	543	5.0
$Pd_{0.1}Zn_1$-10%CNTs	CNTs		6.3	99.8	307	543	5.0
$Pd_{0.1}Zn_1$-10%AC	AC		4.4	99.9	215	543	5.0
$Pd_{0.1}Zn_1$	ZnO		4.1	99.8	202	543	5.0
5%Pd/CNTs	CNTs		4.6	0	0	543	5.0
Rh-ZnO/CNTs	CNTs			96.7	411.4	523	1.0

1.6 Catalyst Preparation

The preparation of the heterogenous catalyst is essential because the activity of the catalyst is highly dependent on the catalyst properties. The two most common types of heterogenous catalyst preparation methods are impregnation and precipitation. The impregnation method involves the support of the catalyst being fabricated to small cylindrical shapes, such as pellets or spheres. The support material is then exposed to a solution that contains either the active compound or a precursor to the active compound. In the precipitation method, the catalyst is prepared by the rapid mixing of the concentrated solutions of metal salts, leading to precipitates with high surface area. The precipitate is then dried and heated to covert the suitable oxides, typically metal oxides, for the active phase.

The most common methanol synthesis catalyst, $Cu/ZnO/Al_2O_3$, is produced on an industrial scale via a co-precipitation method. Co-precipitation is a process in which normally soluble compounds are carried out of solution by a precipitate. For synthesis of $Cu/ZnO/Al_2O_3$ catalyst, the process involves the mixing of metal hydroxy carbonate precursors formed by pH controlled co-precipitation from aqueous Cu,Zn,Al (6:3:1) nitrate solutions and Na_2CO_3 solution as the precipitation agent [19]. The precipitate is then aged in the mother liquor, filtered, washed, dried, and calcined to give the metal oxides. The catalyst is typically provided to the industrial facilities in the oxidized form and must then go through a reduction process typically utilizing the syngas feed as the hydrogen source [19]. Table 1-2 provides an example of typical properties of methanol synthesis catalysts used in industry.

Table 1-2: Typical methanol synthesis catalyst properties provided by Johnson Matthey [8].

Catalyst	KATALCO 51-8	KATALCO 51-8PPT	KATALCO 51-9	KATALCO 51-9S
Form	Solid cylindrical pellets	Solid cylindrical pellets	Solid cylindrical pellets	Solid cylindrical pellets
Diameter (mm)	5.4	5.3	5.3	5.5
Length (mm)	5.2	5.1	5.1	3.65
Typlical loaded density (kg/m^3)	1190	1190	1190	1400-1600

1.7 Catalyst Deactivation

The deactivation mechanisms for traditional catalysts used in industrial scale methanol syntheses, such as CuZnAl, have been widely studied. Catalyst poisoning from contaminants in the syngas feed, Cu particle sintering due to high reaction temperatures, and carbon deposition are the primary mechanisms contributing to deactivation [20]. Catalyst poisons commonly found in syngas include arsine (AsH_3), phosphine (PH_3), hydrogen sulfide (H_2S), carbonyl sulfide (COS), carbon disulfide (CS_2), thiophene (C_4H_4S), methyl thiocyanate (CH_3SCN), methyl chloride (CH_3Cl), and methyl fluoride (CH_3F). Nitrogen-containing species, such as acetonitrile (ACN) and hydrogen cyanide (HCN) have been shown to have little to no effect on catalyst activity, even though the acid/base reaction between ZnO and HCN is thermodynamically favorable. One theory highlighted in the literature suggests HCN undergoes hydrogenation to an inert species, namely methylamine, under the typical methanol synthesis conditions. The reduction in surface area of the catalyst has shown to be approximately linear to the molar concentration of the containment on the catalyst [21].

A recent study conducted by Liang et al. [20] attempted to better quantify the mechanisms using characterization techniques, including X-ray diffraction (XRD), scanning electron microscopy (SEM), and X-ray photoelectron spectroscopy (XPS). The study investigated the performance of $Cu/ZnO/Al_2O_3$ catalyst for CO_2 hydrogenation to methanol over a period of 720 hours. The space time yield (STY) of methanol decreased by 34.5% during the test and samples of the catalyst were taken at different intervals and analyzed. Surprisingly, as Cu aggregation is thought to be main deactivation mechanism, the results showed the Cu particle size did not significantly change during the duration of the test and therefore suggest Cu particle sintering may not be a primary deactivation mechanism. The ZnO particles, however, did undergo significant agglomeration. Previous studies have suggested the water generated during the CO_2 hydrogenation process causes the crystallization of ZnO, directly reducing the overall ZnO surface area and therefore permanently reducing the specific catalyst activity. Although the ZnO particle is not the active site directly involved in the reaction mechanism, segregating the ZnO from the Cu disrupts the SMSI effect needed for high catalyst activity [22].

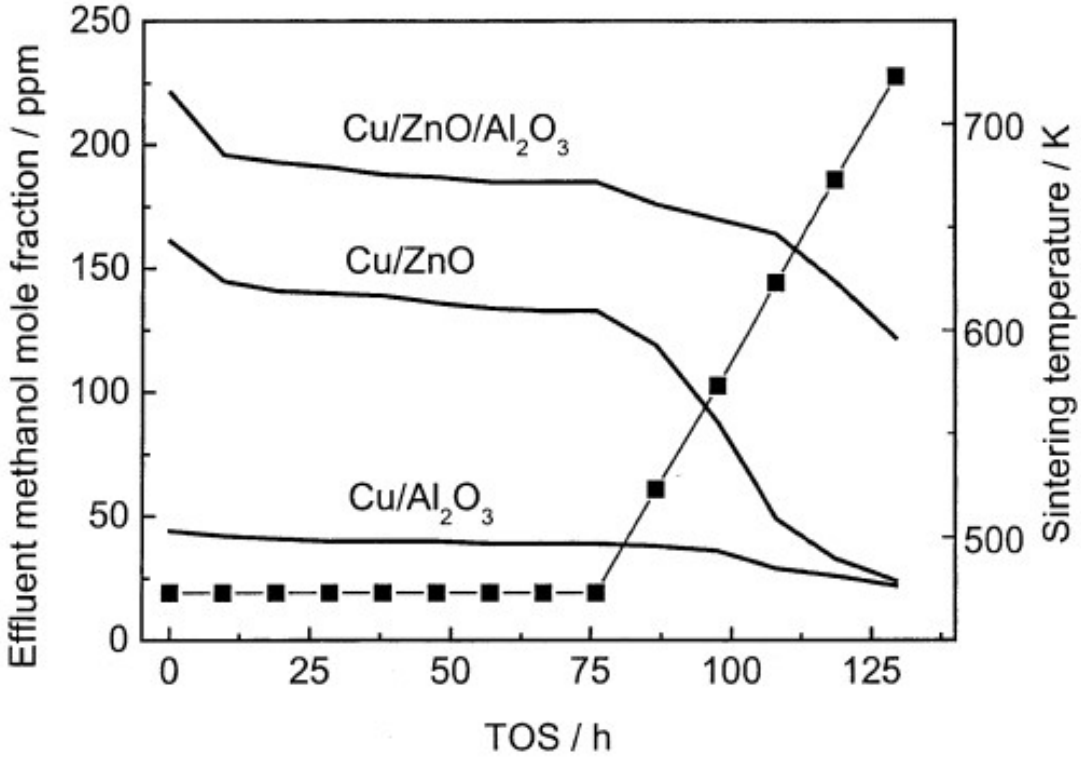

Figure 1-6: Catalyst deactivation behavior influenced by support [23].

The role of the catalyst support and promoter was examined in a study contacted at Ruhr-University Bochum [23]. Cu/ZnO, Cu/Al_2O_3, and Cu/ZnO/Al_2O_3 catalyst samples were prepared and reacted over a 60-day period using a high purity syngas. The results provided in Figure 1-6 show the catalyst without the Al_2O_3 support has a far more pronounced deactivation curve towards the end of the catalyst run. This behavior highlights the role that Al_2O_3 plays as a stabilizer for the Cu crystallites and thus likely inhibits the Cu particles from sintering. The results for the catalyst without the ZnO promoter show relatively stable activity over the test duration; however, the initial activity is significantly lower. This stability highlights the role that ZnO plays in the deactivation process and supports the theory that the ZnO agglomeration is likely the primary deactivation mechanism aside from catalyst poisoning [23].

1.8 Reaction Mechanisms

The general reactions involved in the hydrogenation of CO2 and CO to CH_3OH are as follows:

$$CO + 2H_2 \rightleftarrows CH_3OH \quad \text{(R1)}$$

$$CO_2 + 3H_2 \rightleftarrows CH_3OH + H_2O \quad \text{(R2)}$$

$$CO + H_2O \rightleftarrows H_2 + CO_2 \quad \text{(R3)}$$

The reaction mechanisms involved in the formation of methanol have been studied extensively over the past 50 years and continue to be a source of debate. Early research, notably the work by Natta et al. [24] , considered only the direct hydrogenation of CO as the reaction mechanism involved in methanol synthesis and proposed the following rate equation:

$$r_1 = \frac{f_{CO} f_{H_2}^2 - f_{CH_3OH}/K_1^*}{(A + Bf_{CO} + Cf_{H_2} + Df_{CH_3OH})^3} \quad (1)$$

where f_i denotes the fugacity of component *i* and A, B, C, and D are parameterization constants used to fit the model. This model assumed that the trimolecular reaction between CO and two hydrogen molecules was the rate determining step.

Later work indicated the presence of CO_2 in the feed contributed to the reaction kinetics. Bakemeir et al. [25] continued this analysis and observed that Natta's model deviated from experiment results when the feed was CO_2 rich. Due to this observation, Bakemeir introduced CO_2 dependency into the equation in form of a Langmuir type isotherm:

$$r_1 = \frac{Ae^{-E/RT}[p_{CO}^m p_{H_2}^n (1-(p_{CH_3OH}/p_{CO} p_{H_2}^2 K_1^*))]}{1+De^{-F/RT} p_{CO_2}/p_{H_2}} \quad (2)$$

A, E, m, n, D, and F were determined from experimental data.

The majority of the early reaction mechanisms proposed were modeled using experimental results from methanol synthesis over ZnO/Cr_2O_3 catalyst. This catalyst required the use of high pressure (~300 bar) to overcome the relatively slow kinetics and therefore the models did not accurately predict low pressure conditions. With the development of lower pressure catalysts, namely $Cu/ZnO/Al_2O_3$, additional reaction mechanisms were proposed. Leonov et al. [24] were the first to model methanol synthesis kinetics over a commercial $Cu/ZnO/Al_2O_3$. Their model still assumed CO was the sole carbon source in methanol and the mechanism proposed was primarily a correlative approach.

Later contributions began to focus on the detailed mechanistic considerations in the kinetic model. Klier et al. [26] noticed in his experiments that a maximum was observed in the formation rate while varying the partial pressure ratio of CO to CO_2. The author attributed this phenomenon to the balance between the promoting effect and strong adsorption of CO_2 on the catalyst surface at high concentrations. With a low concentration of CO_2 compared to CO, Klier suggested the catalyst was subject to excessive reduction of the active sites. CO was still considered to the primary carbon source; however, the author now proposed that the number of active sites was directly proportional to the partial pressures of CO and CO_2 through a redox-like mechanism. The following rate equation introduces a new term K^*_{redox} which is intended to represent the equilibrium of this CO/ CO_2 relationship:

$$r_1 = k_1\left(1+\frac{1}{K^*_{redox}}\frac{p_{CO}}{p_{co}}\right)^{-3}\frac{K_{CO}K^2_{H_2}\left(p_{CO}p^2_{H_2}-p_{CH_3OH}/K^*_1\right)}{\left(1+K_{CO}p_{CO}+K_{CO_2}p_{CO_2}+K_{H_2}p_{H_2}\right)} \quad (3)$$

$$r_2 = k_2\left(p_{CO_2}-\frac{1}{K^*_2}\frac{p_{CH_3OH}p_{H_2O}}{p^3_{H_2}}\right) \quad (4)$$

Villa et al. [27] was the first to suggest that a reverse water gas shift (RWGS) reaction must also be considered and proposed the following equation:

$$r_2 = \frac{\left(f_{CO_2}f_{H_2}-f_{CO}f_{H_2O}/K^*_3\right)}{C_6} \quad (5)$$

where K_3^* is the equilibrium constant for the RWGS reaction and C_6 is the constant relative to adsorption equilibrium. He continued the assumption that CO is the only route to methanol and the generation of methanol and the water gas shift reaction occur on different active sites. This new reaction mechanism was derived under the assumption that the reaction between one adsorbed H_2 molecule and one adsorbed CO_2 molecule is rate determining.

It was Graaf et al. [28] who first considered both CO and CO_2 hydrogenation along with the RWGS reaction. The authors suggested a dual site mechanism where CO and CO_2 are adsorbed on a s_1 type site and hydrogen is adsorbed on a s_2 site. Both CO and CO_2 undergo successive hydrogenation while the RWGS occurs via a formate route. The authors did an extensive evaluation on each possible elementary step involved in the three reaction mechanisms. They assumed adsorption and desorption of reactants and products to be in equilibrium and developed 48 possible models by setting each of the elementary steps as the rate limiting steps. Through statistical analysis, the following reaction rate equations were proposed:

$$r_1 = \frac{k'_{ps,A3}K_{CO}\left[f_{CO}f_{H_2}^{3/2} - f_{CH_3OH}/\left(f_{H_2}^{1/2}K_1^*\right)\right]}{\left(1+K_{CO}f_{CO}+K_{CO_2}f_{CO_2}\right)\left[f_{H_2}^{1/2}+(K_{H_2O}/K_{H_2O}^{1/2})f_{H_2O}\right]} \quad (6)$$

$$r_2 = \frac{k'_{ps,C3}K_{CO_2}\left[f_{CO_2}f_{H_2}^{3/2} - f_{CH_3OH}f_{H_2O}/\left(f_{H_2}^{3/2}K_2^*\right)\right]}{\left(1+K_{CO}f_{CO}+K_{CO_2}f_{CO_2}\right)\left[f_{H_2}^{1/2}+(K_{H_2O}/K_{H_2O}^{1/2})f_{H_2O}\right]} \quad (7)$$

$$r_3 = \frac{k'_{ps,B2}K_{CO_2}\left[f_{CO_2}f_{H_2} - f_{H_2O}f_{CO}K_3^*\right]}{\left(1+K_{CO}f_{CO}+K_{CO_2}f_{CO_2}\right)\left[f_{H_2}^{1/2}+(K_{H_2O}/K_{H_2O}^{1/2})f_{H_2O}\right]} \quad (8)$$

where $k'_{ps,A3}$, $k'_{ps,C3}$, and $k'_{ps,B2}$ are pseudo (ps) reaction rate constants containing the adsorption equilibrium constant of hydrogen.

In later work by Vanden Bussche and Froment [24], it was highlighted that the mechanisms proposed by Graaf were fundamentally flawed because the authors failed to account for the fact that some of the intermediates, such as the formyl and methoxy species, are produced

in two different overall reactions, thus implying the model will predict two separate intermediate concentrations for the same species.

The models developed with the assumption that direct hydrogenation of CO and CO_2 are involved in methanol synthesis do not accurately predict catalyst behavior over a wide range of CO_2 concentrations [29]. The work by Vanden Bussche and Froment proposed that CO_2 is assumed to be the only carbon source in methanol [24]. The reaction initiates with CO_2 and H_2 both adsorbing on the active sites of the catalyst, typically copper particles. Carbonate species are then formed by further adsorption of CO_2 and then quickly hydrogenated to bicarbonate and then Cu formate before eventually producing methanol. As indicated in Table 1.2, the hydrogenation of formate is believed to be the rate limiting step and therefore longest living intermediate in the methanol synthesis mechanism.

$$r_2 = \frac{k'_{5a}K'_2K_3K_4K_{H_2}p_{CO_2}p_{H_2}\left[1-(1/K_2^*)\left(p_{H_2O}p_{CH_3OH}/p_{H_2}^3p_{CO_2}\right)\right]}{\left(1+(K_{H_2O}/K_8K_9K_{H_2})(p_{H_2O}/p_{H_2})+\sqrt{K_{H_2}p_{H_2}}+K_{H_2O}p_{H_2O}\right)^3} \quad (9)$$

$$r_3 = \frac{k'_1p_{CO_2}\left[1-K_3^*\left(p_{H_2O}p_{CO}/p_{CO_2}P_{H_2}\right)\right]}{\left(1+(K_{H_2O}/K_8K_9K_{H_2})(p_{H_2O}/p_{H_2})+\sqrt{K_{H_2}p_{H_2}}+K_{H_2O}p_{H_2O}\right)} \quad (10)$$

in which

$$k'_1 = k_1 * c_t \quad (11)$$

$$k'_{5a} = k_{5a} * c_t^2 \quad (12)$$

$$K'_2 = K_2 * c_t \quad (13)$$

Elemental oxygen is released at two stages in the CO_2 hydrogenation process. The oxygen is also hydrogenated by excess hydrogen atoms and water is subsequently produced. This redox process is known as the water gas shift reaction. The rate limiting step for this process is believed to be the dissociative adsorption of CO_2. This reaction is sensitive to temperature

changes and tends to shift towards CO with increasing temperatures. In addition, CO conversion decreases with increasing partial pressures of CO_2 and H_2 and increases with increasing water partial pressure or decreasing CO partial pressure [30].

Table 1-3: Theoretical mechanism scheme proposed by Vanden Bussche and Froment [24].

H_2 (g) + 2s	⇆	2 H.s	K_{H2}	
CO_2 (g) + s	⇆	O.s + CO (g)	k_1,K_1	RDS
CO_2 (g) + O.s + s	⇆	CO_3.2s	K_2	
CO_3.2s + H.s	⇆	HCO_3.2s + s	K_3	
HCO_3.2s + s	⇆	HCO_2.2s + O.s	K_4	
HCO_2.2s + H.s	⇆	H_2CO_2.2s + s	K_{5a}	RDS
H_2CO_2.2s	⇆	H_2CO.s + O.s	K_{5b}	
H_2CO.s + H.s	⇆	H_3CO.s + s	K_6	
H_3CO.s + H.s	⇆	CH_3OH (g) + 2s	K_7	
O.s + H.s	⇆	OH.s + s	K_8	
OH.s + H.s	⇆	H_2O.s + s	K_9	
H_2O.s	⇆	H_2O (g)+ s	K_{H2O}	

RDS = Rate Determining Step

1.9 Thermodynamics

1.9.1 Chemical Equilibria

Given the high-pressure reaction conditions and the presence of polar molecules, some of which are below their critical temperatures, the equilibrium expressions can be influenced by non-ideal behavior. The equilibrium constants for the three reactions (11) (12) (13) involved in methanol synthesis can be expressed as:

$$K_{f1} = \left(\frac{f_{CH_3OH}}{f_{CO} f_{H_2}^2}\right)_{Eq} = \left(\frac{\varphi_{CH_3OH}}{\varphi_{CO}\varphi_{H_2}^2}\right)_{Eq} \left(\frac{p_{CH_3OH}}{p_{CO} p_{H_2}^2}\right)_{Eq} = K_{\varphi 1} K_1^* \quad (14)$$

$$K_{f2} = \left(\frac{f_{CO} f_{H_2O}}{f_{CO_2} f_{H_2}}\right)_{Eq} = \left(\frac{\varphi_{CO}\varphi_{H_2O}}{\varphi_{CO_2}\varphi_{H_2}}\right)_{Eq} \left(\frac{p_{CO} p_{H_2O}}{p_{CO_2} p_{H_2}}\right)_{Eq} = K_{\varphi 2} K_2^* \quad (15)$$

$$K_{f3} = K_{f1} K_{f2} \quad (16)$$

where f_i is the fugacity of component i and φ_i is the fugacity coefficient. The values for $K_{\varphi 1}$ and $K_{\varphi 2}$ must be determined by using an equation of state, however, at low pressures, most gases exhibit ideal gas behavior and therefore the following assumption can be made at atmospheric pressure:

$$K_f = K^* \quad (17)$$

K^* can then be estimated as a function of temperature only using the following thermodynamic relationships:

$$-\Delta G^{\circ}(T) = RT \ln K^* \quad (18)$$

$$\frac{-\Delta G^{\circ}(T)}{T} = \frac{-\Delta G^{\circ}(T_{ref})}{T_{ref}} - \int_{T_{ref}}^{T} \frac{\Delta H^{\circ}(T)}{T^2} dT \quad (19)$$

$$\Delta H^{\circ}(T) = \Delta H^{\circ}(T_{ref}) + \int_{T_{ref}}^{T} \Delta C_p^{\circ}(T)\, dT \quad (20)$$

K^* becomes solely a function of heat capacities which are polynomial functions of T. For a relatively small temperature range, the following simplification can be derived:

$$\log_{10} K^* = \frac{b_1}{T} + b_2 \quad (21)$$

where b_1 and b_2 are determined using the specific heat data and reference heats of formation and Gibbs free energy values. Graaf et al. [31] obtained the following simplified equations in his work:

$$log_{10} K_1^* = \frac{5139}{T} - 12.621 \quad (22)$$

$$log_{10}\, 1/K_2^* = -\frac{3066}{T} - 10.592 \quad (23)$$

$$log_{10}\, K_3^* = -\frac{2073}{T} + 2.029 \quad (24)$$

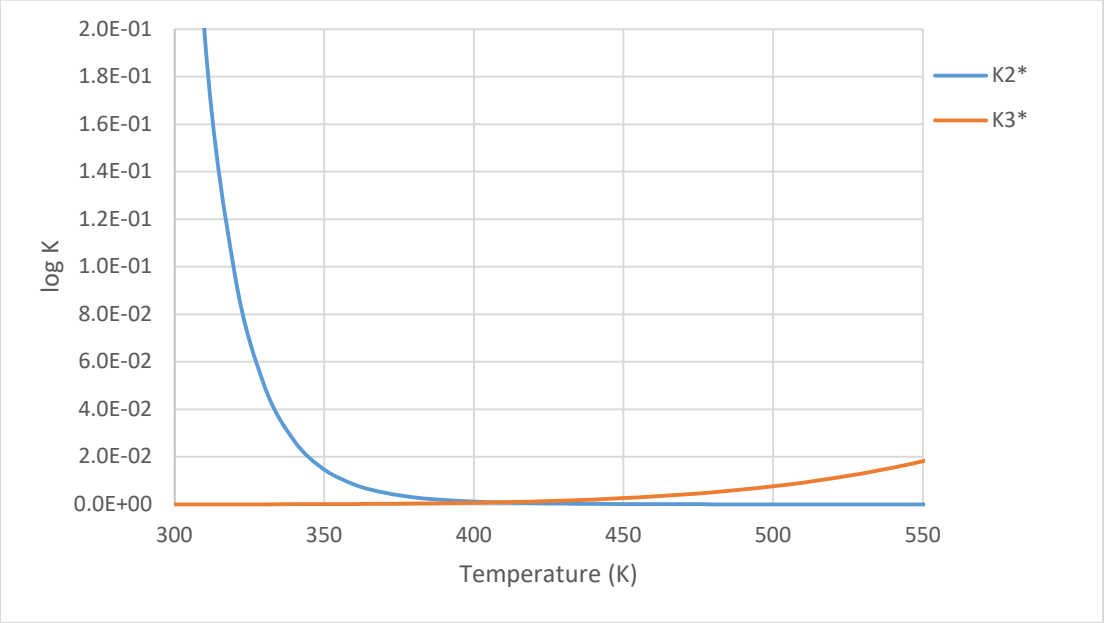

Figure 1-7: Equilibrium constants for reaction (2) and reaction (3) as a function of temperature.

Figure 1-7 shows the temperature dependence of the equilibrium constants for reactions (2) and (3) considered in this work. The RWGS reaction (3) is not significantly influenced by temperature.

The fugacity of component *i* is determined by the following:

$$f_i = y_i \varphi_i^V P \tag{25}$$

where φ_i^V is determined by using an equation of state.

1.9.2 Thermodynamic Model

The Peng-Robinson equation of state (EOS) was chosen for this work due to its inherent use in the petroleum and chemical industry [32]. The model was developed in the 1970's by the University of Alberta in Canada and the work was sponsored by the Canadian Energy Board for use for natural gas systems. This EOS is thought to be a slight improvement to the Soave-Redlich-Kwong EOS developed just a few years prior, particularly for components around their critical points.

The pressure explicit Peng Robinson equation of state is written as:

$$P = \left(\frac{RT}{\bar{V}-b}\right) - \left(\frac{a_i(T)}{\bar{V}(\bar{V}+b)+b(\bar{V}+b)}\right) \tag{26}$$

where

$$\alpha = (1 + k(1 - \sqrt{T_r}))^2 \tag{27}$$

$$a = a_c \alpha \tag{28}$$

$$k = 0.37464 + 1.54226\omega - 0.26992\omega^2 \tag{29}$$

$$a_c = 0.45724 \frac{R^2 T^2}{P_c} \tag{30}$$

$$b = 0.0778 \frac{RT}{P_c} \tag{31}$$

$$T_r = \frac{T}{T_c} \tag{32}$$

1.10 Limitations of Previous Studies

Significant research has been done on modeling the kinetic behavior of the methanol synthesis reactions. This knowledge has allowed industry to make substantial process improvements that has kept methanol at the forefront of viable energy sources as we find solutions to reduce greenhouse gas emissions. However, much of the prior analysis focuses on lower pressures (<55 bar) and high temperatures (> 500K) than many of the industrial applications used today. The vast majority of the ICI low pressure processes operate up to 125 bar with inlet temperatures as low as 400 K [10]. A recent study investigated the use of much higher pressures (170-200 bar) to produce ultra-pure methanol using $Cu/ZnO/Al_2O_3$ catalyst, however, the results were not considered in this work given the pressure range far exceeds the feasible operating conditions used in most industrial processes operating today.

The kinetic studies reviewed in the literature review were largely performed with significantly lower stoichiometric number (SN) than typically found in industrial methanol synthesis processes. SN is defined as:

$$SN = \frac{y_{H_2} - y_{CO_2}}{y_{CO} + y_{CO_2}} \tag{33}$$

As noted by Nester et al. [6], excess H_2 produced from the steam reforming process is often recycled to the reactor feed to prevent byproduct formation. A better understanding of the impact of this increase in the H2 partial pressure on the reaction kinetics needs to be demonstrated using typical industrial methanol synthesis process conditions.

The effects of non-ideal gas behavior on methanol synthesis is scarcely available in the published literature [31], especially for the higher pressure and lower temperature operating conditions found with most industrial scale methanol processes. The work by Graaf et al. [28] mentions the use of the Soave-Redlich-Kwong equation of state in the development of the model but does not provide any detail on the deviation from ideality or the significance of such occurrence. Later work by Froment et al. [24], which is widely considered a vital paper describing methanol synthesis kinetics, does not address the effects of non-ideality in their work.

In fact, it appears by the direct use of partial pressures instead of fugacity in his proposed reaction rate equations that the author is neglecting this all together. It is noted that both the work by Graaf and Froment were based on substantially lower pressures and high temperatures than used in industry and therefore the effects of non-ideality in their work are likely less important.

1.11 Research Objectives

Given these limitations identified in the literature review, the following analysis was performed to improve on the extensive historical knowledge of methanol synthesis technology by conducting a detailed kinetic analysis using typical operating conditions of a ICI low pressure methanol process. The effects of temperature, pressure, and composition are examined as well as the effects of non-ideality using the Peng-Robinson equation of state. This deeper understanding of kinetic behavior is imperative to developing feasible opportunities to utilize methanol synthesis in the fight to reduce CO_2 emissions.

Chapter 2 - Simulation

2.1 Model Development

A steady state one-dimensional mathematical model was developed in MATLAB for a single pass methanol synthesis reactor. The model utilizes the ODE45 solver to solve the ordinary differential equations used for the mole balance, pressure drop, and temperature profiles. It is noted that the ODE45 solver was unable to converge over the entire parameter range with the thermodynamic analysis included. This was likely due to model stiffness given the model's complexity. For this case, ODE23 was utilized as it can withstand a higher degree of stiffness although can produce less accurate results. A sensitivity analysis was performed using both solvers for the model without thermo effects over the entire parameter range and the results were within 0.1% of each other. The following assumptions were also incorporated:

- Negligible axial dispersion
- Maximum radial mixedness due to the small ratio of reactor diameter to reactor length and thus a one-dimensional model.
- Pseudo-homogeneous and uniform catalytic particles with constant temperature and pressure profiles within the catalyst pellets
- Negligible catalyst deactivation for the operating parameters analyzed in this study.
- Negligible side reactions except for the RWGS reaction due to high catalyst selectivity.
- Pseudo-homogeneous model: Gradients between gas and solid phase are neglected due to the small size of catalyst particles.

2.2 Physical Parameters

Reactor

Diameter – 0.25 m

Length – 2.5 m

Catalyst

Weight – 1 kg
Density – 1190 kg/m^3
Porosity – 0.4

Feed Stream

Table 2-1: Typical syngas feed composition used in methanol production [6].

Component	Feed Rate (mol/s)	Composition (mole %)
CO2	0.0002	1.50%
Hydrogen	0.0085	85.00%
CO	0.0003	3.00%
Methane	0.0011	10.50%

2.3 Kinetics

The reaction rate equations proposed by Vanden Bussche and Froment were chosen for this simulation due to previously demonstrated accuracy over other models [6].

$$r_2 = \frac{K'_{5a}K'_2K_3K_4K_{H_2}p_{CO_2}p_{H_2}\left[1-(1/K_2^*)\left(p_{H_2O}p_{CH_3OH}/p_{H_2}^3p_{CO_2}\right)\right]}{\left(1+\left(K_{H_2O}/K_8K_9K_{H_2}\right)\left(p_{H_2O}/p_{H_2}\right)+\sqrt{K_{H_2}p_{H_2}}+K_{H_2O}p_{H_2O}\right)^3} \quad (34)$$

$$r_3 = \frac{k'_1p_{CO_2}\left[1-K_3^*\left(p_{H_2O}p_{CO}/p_{CO_2}P_{H_2}\right)\right]}{\left(1+\left(K_{H_2O}/K_8K_9K_{H_2}\right)\left(p_{H_2O}/p_{H_2}\right)+\sqrt{K_{H_2}p_{H_2}}+K_{H_2O}p_{H_2O}\right)} \quad (35)$$

Table 2-2: Kinetic parameters determined by Vanden Bussche and Froment [24].

K1A	0.499
K1B	17197
K2A	6.62E-11
K2B	6.62E-11
K3A	3453.38
K3B	1
K4A	1.07
K4B	36696
K5A	1.22E10
K5B	-94765

The kinetic parameters used in this model were determined using an experimental data set based on a maximum pressure of 50 bar. This is expected to produce a deviation between the simulated results and actual kinetic performance, however, the general trends in kinetic behavior shown from this simulation are expected to be valid. The kinetic parameters were corrected for temperature using the following equation:

$$K_i = K_{iA} * exp(K_{iB}/(R*T)); \quad (36)$$

The equilibrium constants used in the model were determined by the work by Graaf et al. [31] as provided in section 1.9.1. The ideal temperature corrected equilibrium constants determined from the equations below were corrected for non-ideality using the Peng-Robinson equation of state.

$$log_{10}K_2^* = 3066/T - 10.592 \quad (37)$$

$$log_{10}1/K_3^* = -2073/T + 2.029 \quad (38)$$

2.4 Pressure Drop

Pressure drop across the packed bed reactor was estimated using the Ergun equation. The pressure drop is a function of catalyst and stream properties [33].

$$\frac{dP}{dW} = -\frac{\alpha}{2}\frac{T}{T_0}\frac{P_0}{\frac{P}{P_0}}\left(\frac{F_T}{F_{T0}}\right) \tag{39}$$

$$\alpha = \frac{2\beta_0}{A_c\rho_c(1-\theta)P_0} \tag{40}$$

$$\beta_0 = -\frac{G(1-\theta)}{\rho_0 g_c D_p \theta^3}\left[\frac{150(1-\theta)\mu}{D_p} + 1.75G\right] \tag{41}$$

2.5 Energy Balance

$$\frac{dT}{dW} = \frac{U*a*(T_a-T)+(-r_1)(-\Delta H_{rxn1})+(-r_2)(-\Delta H_{rxn2})}{F_{CO2}C_{p_{CO}} + F_{H_2}C_{p_{H_2}}+F_{CH_3OH}C_{p_{CH_3OH}}+F_{H2o}C_{p_{H2o}}+F_{CO}C_{p_{CO}}+F_{CH_4}C_{p_{CH_4}}} \tag{42}$$

$$\Delta H_{rxn1} = -49.5 * 10^3 + \Delta C_{p_{rxn1}} \tag{43}$$

$$\Delta H_{rxn2} = 41.2 * 10^3 + \Delta C_{p_{rxn2}} \tag{44}$$

$$\Delta C_{p_{rxn1}} = C_{p_{CH3OH}} + C_{p_{H20}} - 3 * C_{p_{H2}} - C_{p_{CO2}} \tag{45}$$

$$\Delta C_{p_{rxn2}} = C_{p_{H2}} + C_{p_{CO2}} - C_{p_{CO}} - C_{p_{H20}} \tag{46}$$

$$a = 4/(D_t * (1-\theta) * \rho_c) \tag{47}$$

U = 0 for adiabatic operation

2.6 Mole Balance

$$\frac{dF_{CO2}}{dW} = -r_1 - r_2 \quad (48)$$

$$\frac{dF_{H2}}{dW} = -3r_1 - r_2 \quad (49)$$

$$\frac{dF_{CH3OH}}{dW} = r_1 \quad (50)$$

$$\frac{dF_{H2O}}{dW} = r_1 + r_2 \quad (51)$$

$$\frac{dF_{CO}}{dW} = r_2 \quad (52)$$

$$\frac{dF_{CH}}{dW} = 0 \quad (53)$$

Chapter 3 - Model Results and Discussion

3.1 Effects of Temperature and Pressure

Figure 3.1 shows that temperature has a negative effect and pressure has a positive effect on the carbon dioxide conversion to methanol. This behavior is expected and can be explained by Le Chatelier's principle for exothermic reactions. In equilibrium reactions, an increase in temperature decreases the equilibrium constant and therefore the equilibrium favors the reactants. An increase in pressure has the opposite effect as the equilibrium concentrations directly rely on partial pressures of the products and reactants. Relatively high conversion CO_2 conversion to methanol (~ 73%) was predicted at 120 bar and 450 K, which were the extremes tested in this analysis. The effects of temperature and pressure were analyzed using a typical stoichiometric CO_2-H_2 ratio of (1:43) and CO-CO_2 ratio of (3:2) in the feed stream.

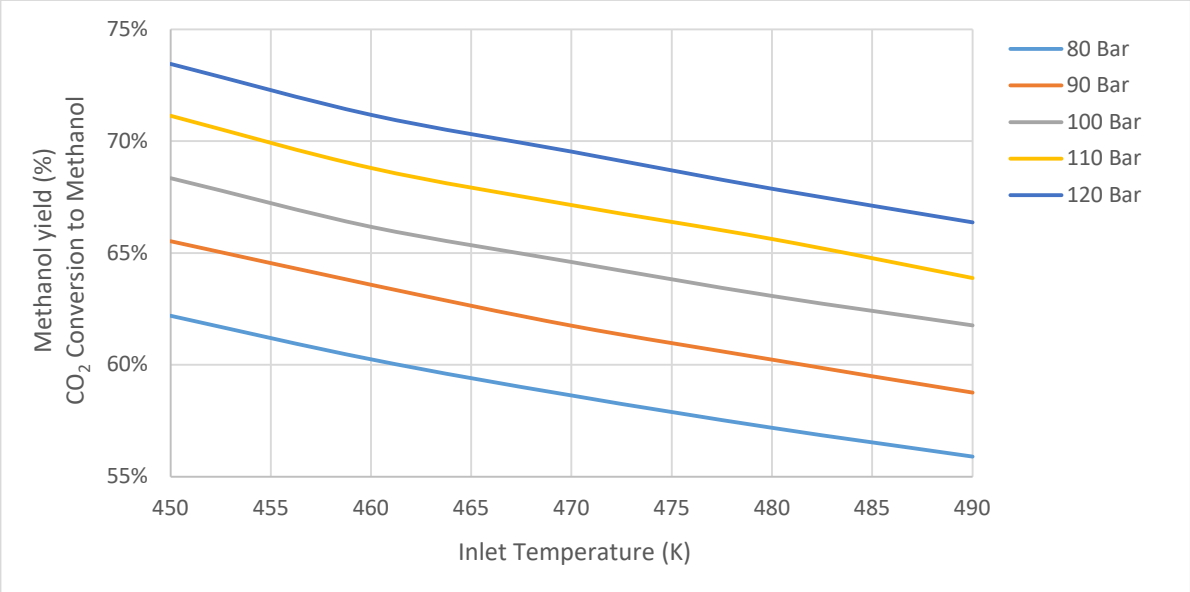

Figure 3-1: Equilibrium CO_2 conversion to methanol and methanol yield as a function of temperature and pressure.

The global CO_2 conversion as a result of both reaction 1 and reaction 2 was analyzed at thermodynamic equilibrium, as shown in Figure 3.2. As expected, global CO_2 conversion also

decreases with temperature, however, the decrease is more pronounced than only CO_2 conversion to methanol. Figure 3.3 compares CO_2 conversion to methanol to the overall CO_2 conversion. As the temperature increases, the endothermic RWGS reaction equilibrium will shift towards the formation of CO and H_2O and therefore no additional CO_2 is being generated for use in the hydrogenation reaction. At 490K, only CO_2 from the feed is being converted to methanol.

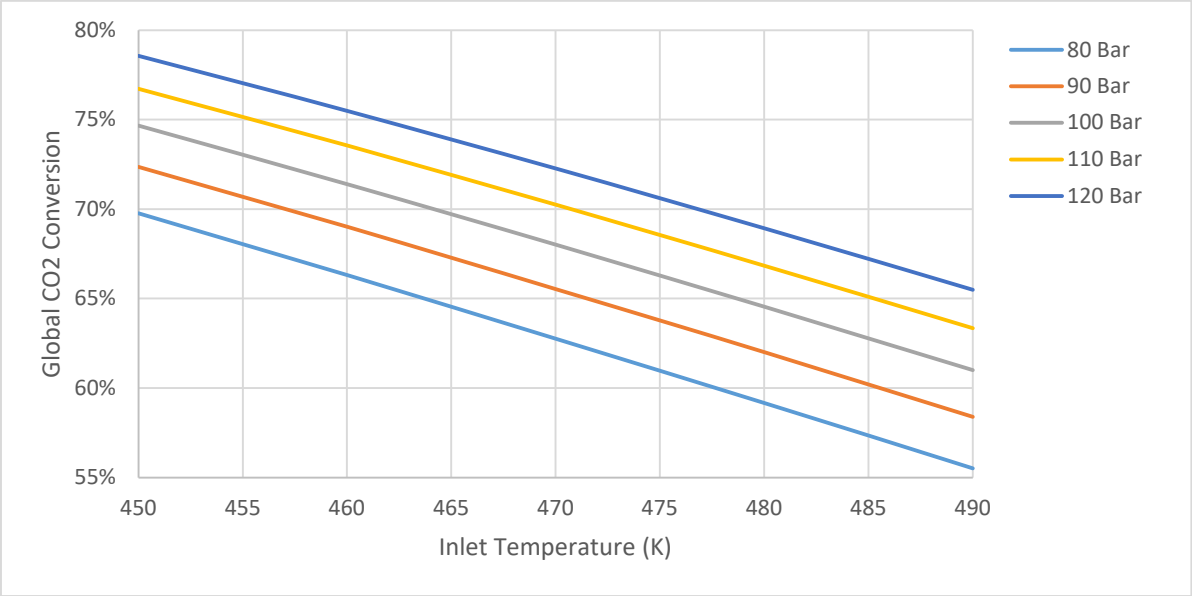

Figure 3-2: Overall CO_2 conversion at equilibrium conditions as a function of temperature and pressure.

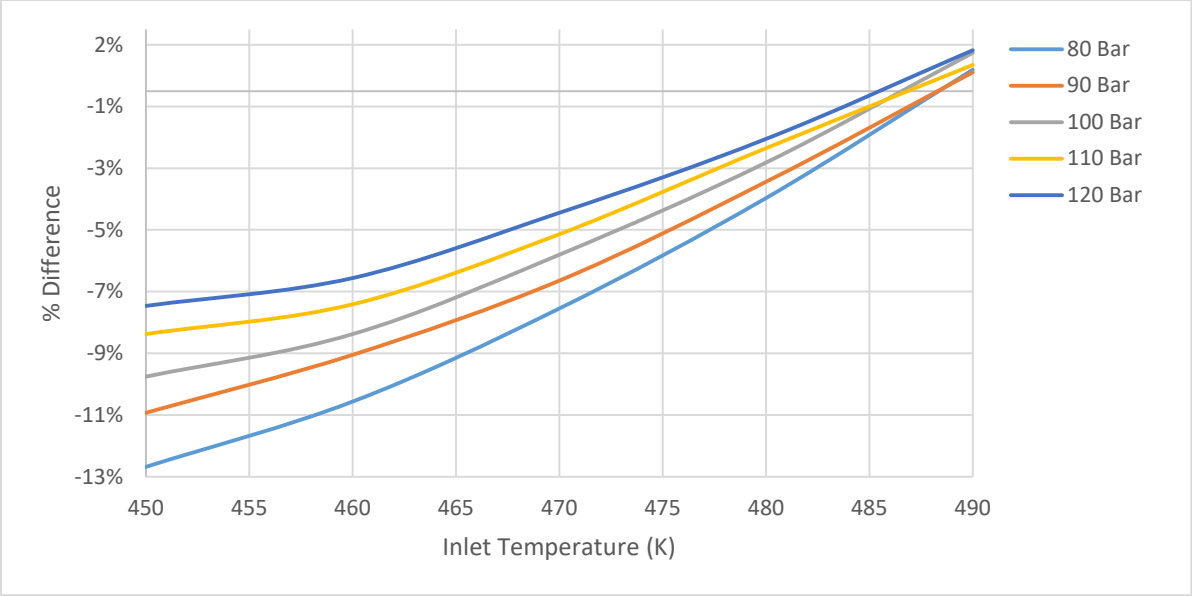

Figure 3-3: Percent difference between CO_2 conversion to methanol and global CO_2 as a function of temperature and pressure.

3.2 Effects of CO/CO_2 in Feed

The presence of CO in the syngas has been reported to increase global CO_2 conversion to methanol [29]. Under the conditions used in this simulation and typical industrial scale methanol synthesis processes, the opposite effect was observed. The carbon oxide ratio (COR) is defined as:

$$COR = \frac{CO_2}{CO_2+CO} \tag{54}$$

As shown in Figure 3-4, the highest global CO_2 conversion was obtained using only CO_2 (COR = 1) with a constant SN of 14. The RWGS reaction progresses slower than the methanol synthesis reaction and therefore given the high H_2 content under the simulated conditions, the RWGS equilibrium is pushed towards CO and H_2O production. The CO in the feed would have to increase substantially, beyond the range analyzed in this study, to overcome the H_2 and push the equilibrium in the opposite direction and thus freeing up CO_2 for synthesis.

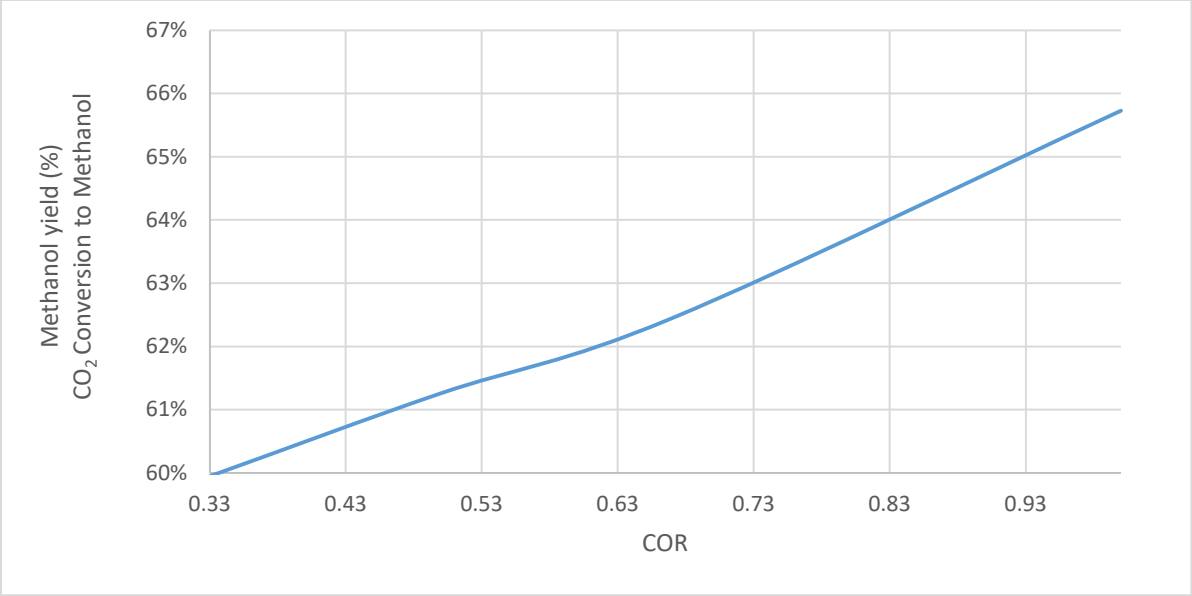

Figure 3-4: Equilibrium methanol yield and global CO_2 conversion to methanol as a function of carbon oxide ratio (COR) at constant pressure (T_0 = 475K, P_0 = 100 bar).

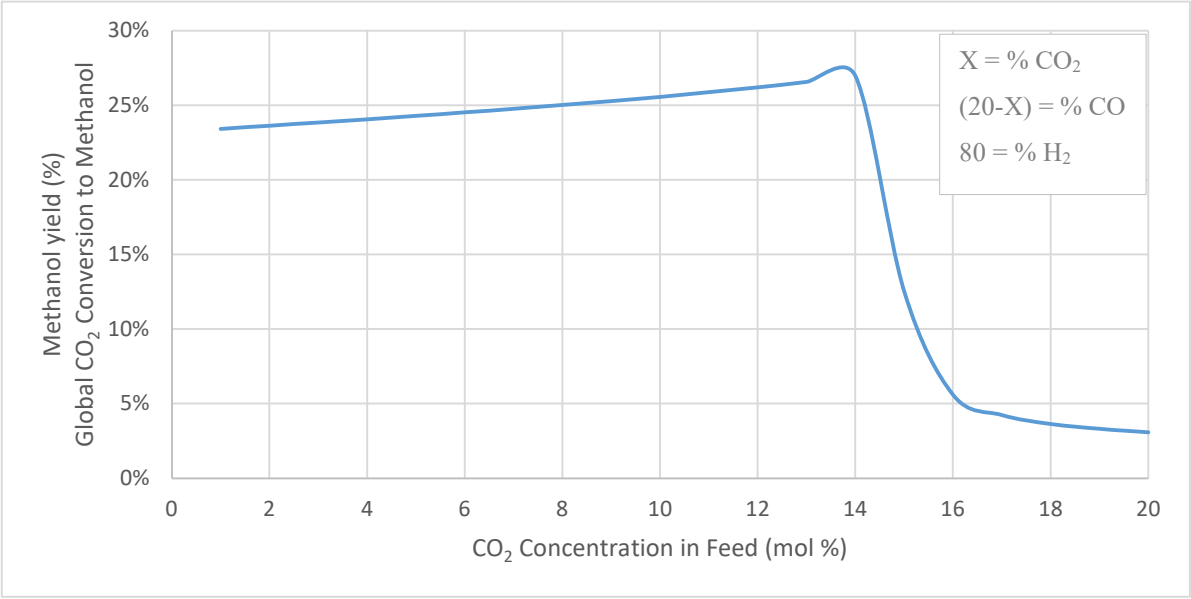

Figure 3-5: Equilibrium methanol yield and global CO_2 conversion to methanol as a function of CO_2 concentration (T_0 = 475K, P_0 = 100 bar).

Figure 3-5 further highlights this phenomenon using a constant H_2 concentration (SN 3-4). As the CO_2 concentration increases, a maximum is reached at which time the RWGS reaction reaches equilibrium and drastically reverses direction. Vanden Bussche et al. ascribes this behavior as a result of excess H_2O formation that eventually slows the methanol synthesis reaction. At this point, it becomes advantageous to have CO in the feed, although CO_2 in excess of ~2% is typically not used in order to ensure high conversion is obtained [6]. The effect of COR on conversion while maintaining a SN of 14 is shown in Figure 3-6. COR has a more pronounced effect as the pressure is increased with maximum again obtained with CO present in the feed.

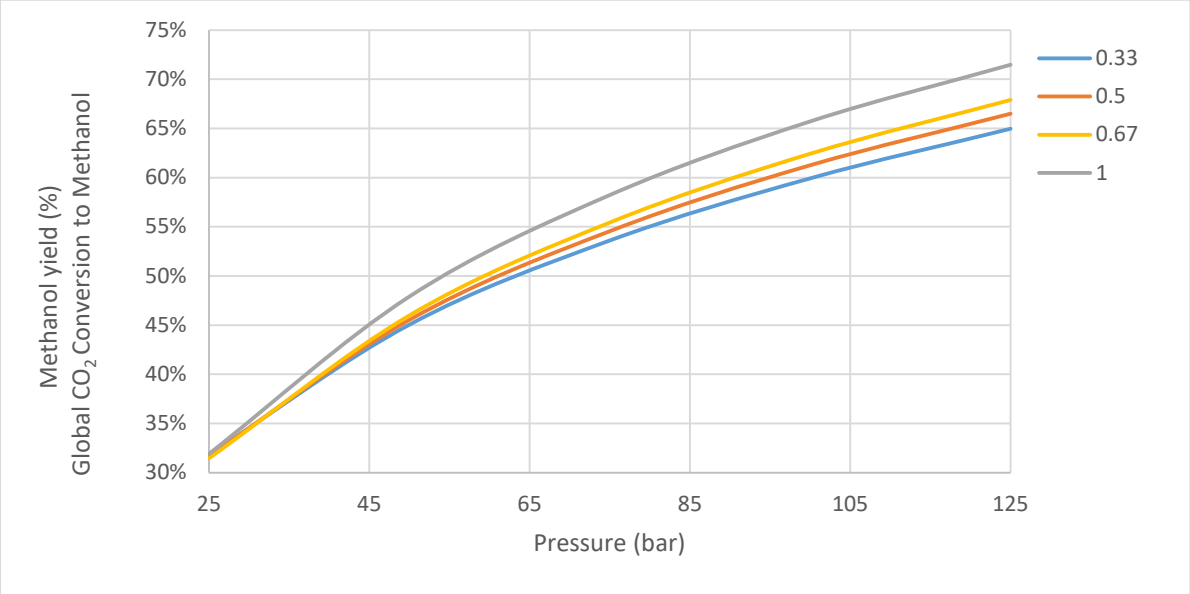

Figure 3-6: Equilibrium methanol yield and global CO_2 conversion to methanol as a function of pressure at different COR values from 0.33 to 1 (T_0 = 475K).

3.3 Effects of H_2 in Feed

The role of hydrogen content in the feed and its effect on methanol synthesis is demonstrated by Figures 3-7 and 3-8. The effluent concentrations were predicted using a constant COR of 0.4 with varying H_2 content in the feed. A H_2 concentration less than 25 percent results in the RWGS shift reaction (3) proceeding to produce excess CO_2 and therefore increases the rate of CH_3OH formation. At 25 percent, the RWGS reaction (3) begins to reach equilibrium

and subsequently the CO concentration stabilizes. At 75% H_2, only CO_2 in the feed is being converted to CH_3OH. A steeper rate of CH_3OH formation is observed due to the equilibrium push from the increased H_2% per the methanol synthesis reaction (2).

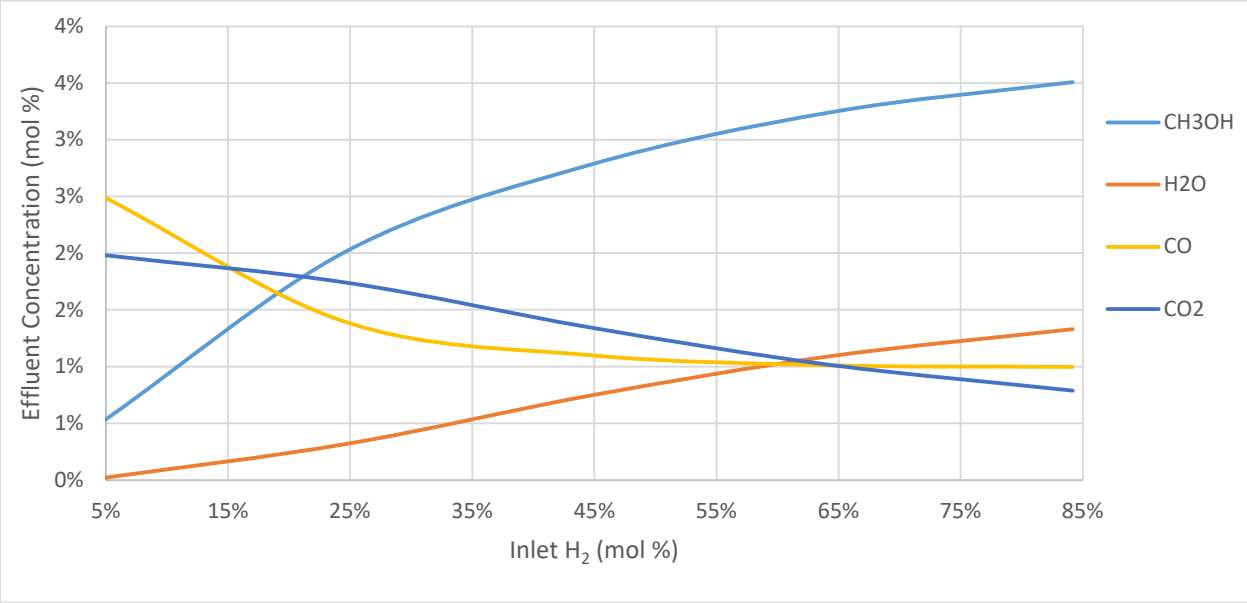

Figure 3-7: Reactor effluent concentrations as a function of H_2 in feed (T_0 = 475K, P_0 = 100 bar).

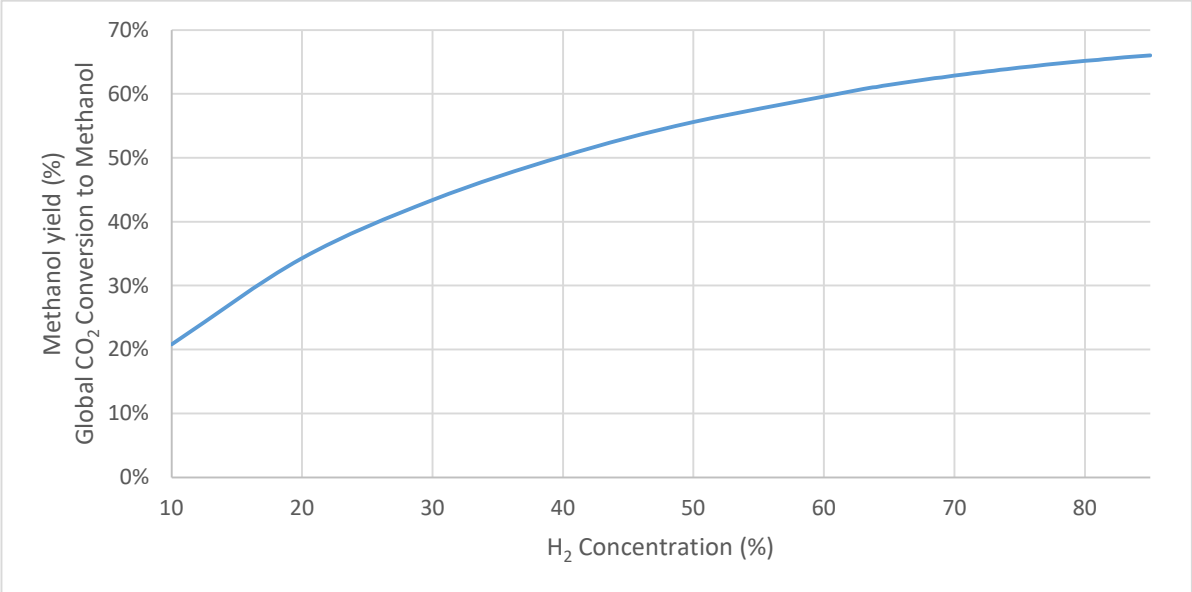

Figure 3-8: Equilibrium methanol yield and global CO_2 conversion to methanol as a function of H_2 concentration (T_0 = 475K, P_0 = 100 bar).

3.4 Pressure Drop Effects

Pressure drop across a packed bed reactor was simulated using the properties of commercial methanol synthesis catalyst as well as typical industrial process conditions. Reactor configurations vary depending on the technology, so this analysis assumes a standard singe pass reactor with a height to diameter ratio of 2.5. The typical porosity of fresh methanol synthesis catalyst ranges from 0.3 to 0.5. The results as shown in Figure 3-8 suggest that pressure drop is not a major factor in traditional packed bed designs without the presence of fouling, although a more substantial impact may be observed in internally cooled tubular reactor designs. It is noted that this simulation considered the catalyst properties to remain constant and therefore did not incorporate the presence of fouling. Significant fouling, such as sintering, can change the catalyst particle size and porosity and therefore can lead to a high pressure drop.

Pressure drop as a function of gas hourly space velocity (GHSV) was simulated with the same properties stated in the previous paragraph while varying the flow rate. The flow rate was varied to simulate the typical range of GHSV used for industrial scale methanol synthesis processes [34]. Figure 3-9 shows a ~1 percent pressure drop is observed at a GHSV of 10,000 hr^{-1}, a typical design parameter for packed bed reactors. Although pressure drop is more sensitive to GHSV than catalyst diameter under these conditions, CO_2 conversion doesn't become significantly impacted until a GHSV greater than 30,000 hr^{-1} (% ΔP ~10%).

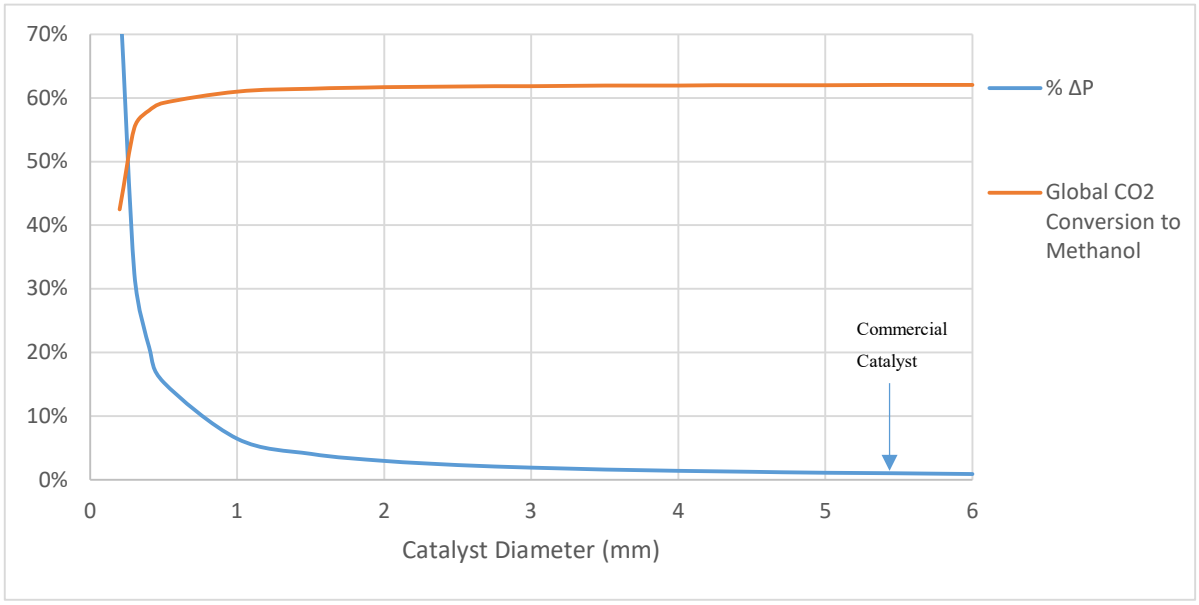

Figure 3-9: Pressure drop and CO_2 conversion as a function of catalyst pellet size (T_0 = 475K, P_0 = 100 bar).

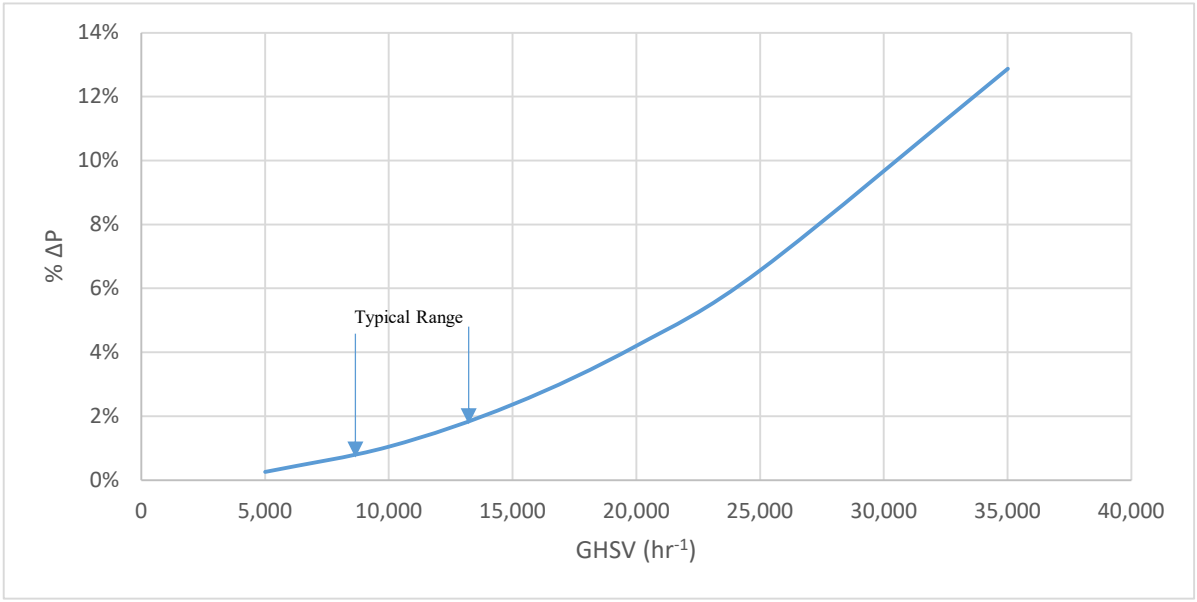

Figure 3-10: Pressure drop as a function of GHSV with typical industrial process conditions (T_0 = 475K, P_0 = 100 bar).

3.5 Effects of Non-Ideality on Reactor performance

This reactor model incorporated the Peng Robinson equation of state to simulate the effects of non-ideality on reactor performance. Figure 3-10 shows the results of a model simulation using the Ideal EOS vs. the Peng Robinson EOS. As shown by the results, there is approximately a five percent increase in the predicted CO_2 conversion to CH_3OH for the non-ideal model versus ideal. This can be explained by the decrease in partial pressure for polar reaction products CH_3OH and H_2O as a result of the reduction in fugacity coefficients as shown in Table 3-1. The reduced partial pressures push the equilibrium for the methanol synthesis reaction towards increased CH_3OH and H_2O formation via reaction (2) and therefore a higher CO_2 conversion to CH_3OH. Consequently, the reduction in H_2O partial pressure pushes the RWGS reaction (3) towards the formation of CO and H_2O and therefore a decrease in CO_2 available for methanol synthesis. This results in the global CO_2 conversion to move closer to the feed CO_2 conversion as the CO equilibrium to CO_2 is reduced.

Table 3-1: Fugacity coefficients at reactor outlet

CO_2	0.9813
H_2	1.0340
CH_3OH	0.9181
H_2O	0.8916
CO	1.0449
CH_4	1.0145

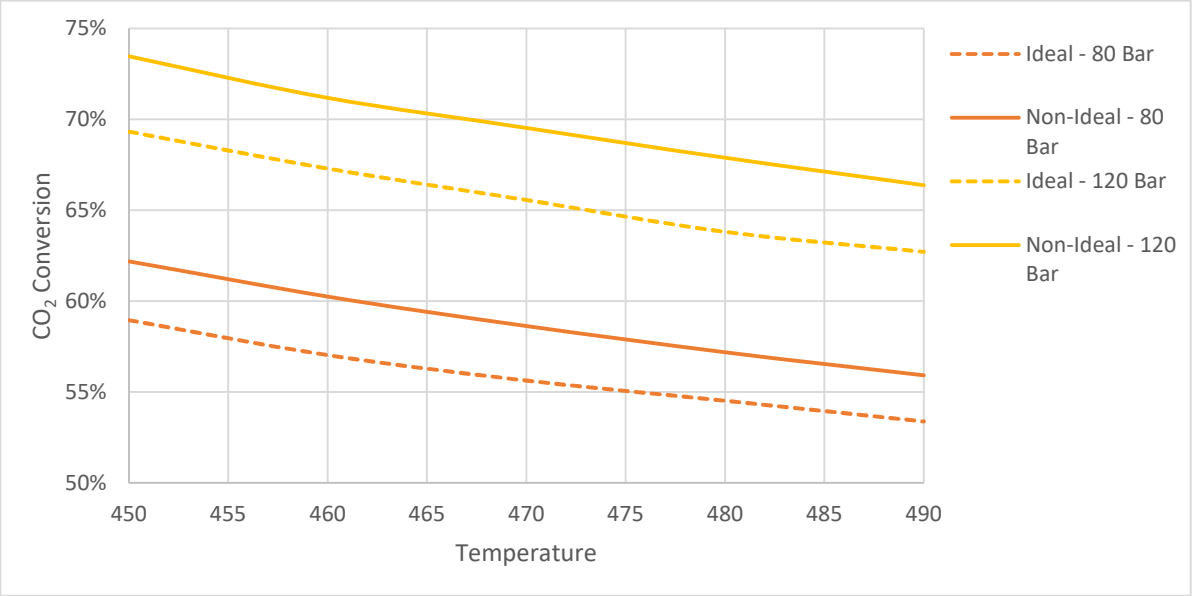

Figure 3-11: Effects of non-ideality on CO_2 conversion to methanol as a function of temperature at different inlet pressures.

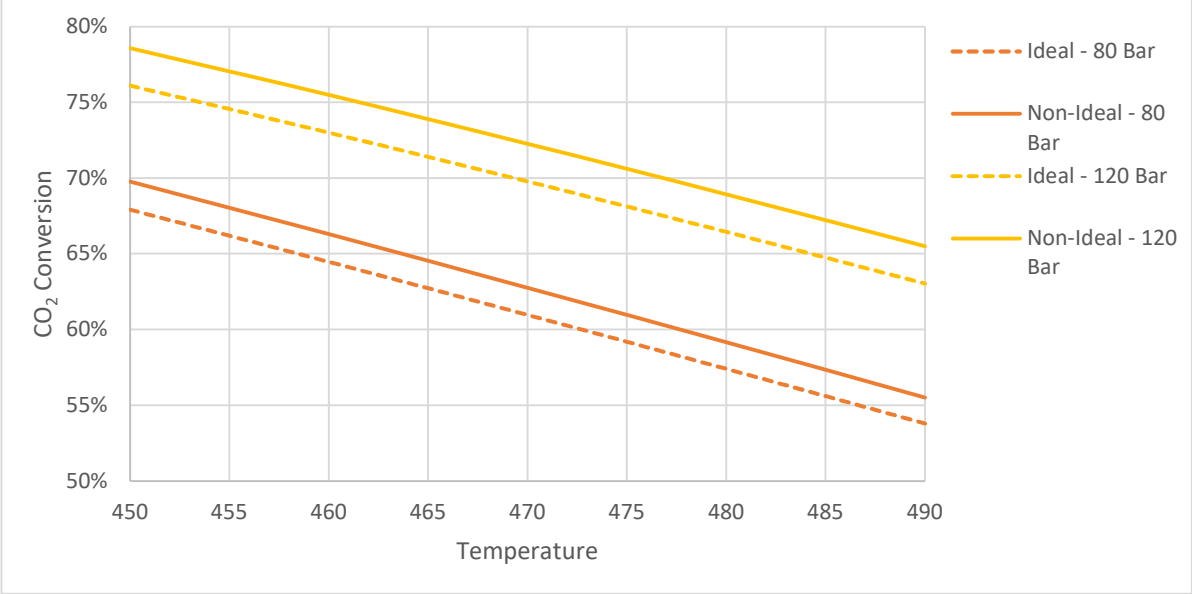

Figure 3-12: Effects of non-ideality on global CO_2 conversion as a function of temperature at different inlet pressures.

3.6 Conclusion and Future Work

This work explores the development of methanol synthesis catalyst including a thorough literature review of catalyst properties, deactivation, and kinetic mechanisms. The catalytic performance of $Cu/ZnO/Al_2O_3$ catalyst was explored using a kinetic model developed in MATLAB. The results highlight the negative effect that CO in the feed has on conversion at high H_2 to CO_2 ratios. Pressure drop across a packed bed reactor using typical industrial conditions was also simulated and determined to be negligible for typical reactor configurations and catalyst properties. The effects of non-ideality on reactor performance were simulated using industrial methanol synthesis conditions. The results show up to a 5 percent increase in CO_2 conversion is predicted when including thermodynamic effects in the reactor simulation. This phenomenon can be explained by the reduction of partial pressure of the products formed via the methanol synthesis reaction and therefore a shift in equilibrium towards methanol production.

The goal of this research is to highlight the fundamental kinetic behavior of current methanol synthesis catalysts using reactor conditions currently utilized in industry. This deeper understanding is critical to being able to optimize the existing infrastructure to help convert unwanted CO_2 emissions to a viable energy carrier and subsequent products. A key limitation of this work is the lack of experimental data sets available using typical industrial conditions, likely due to physical limitations of bench scale reactors. This data is necessary to tune the kinetic parameters of the model and improve the accuracy of the simulation over broad process conditions. Future work should also include a detailed analysis of heat transport phenomena in a packed bed reactor using methanol synthesis catalyst. While alumina has been shown to provide additional benefits beyond an inert support, as explained in this report, novel support material with higher thermal conductivity, such as CNTs, may offer potential improvements over existing catalyst technology.

References

[1] EPA. "Overview of Greenhouse Gases." Environmental Protection Agency. https://www.epa.gov/ghgemissions/overview-greenhouse-gases#carbon-dioxide (accessed.

[2] Q. Tan, Z. Shi, and D. Wu, "CO2 Hydrogenation to Methanol over a Highly Active Cu-Ni/CeO2 Nanotube Catalyst," *Industrial & Engineering Chemistry Reserach,* vol. 57, pp. 10148-10158, 2018.

[3] (2019). *Putting CO2 to Use: Creating Value From Emissions*.

[4] "Putting CO2 to Use: Creating Value From Emissions," IEA, 2019.

[5] "Evaluation of the Fate and Transport of Methanol in the Environment," American Methanol Institute, Washington, DC, 1999.

[6] F. Nestler *et al.*, "Kinetic Modeling of Methanol Synthesis Over Commercial Catalysts: A Critical Assessment," *Chemical Engineering Journal,* vol. 394, 2020.

[7] R. Cho, "Capturing Carbon's Potential: These Companies are Turning CO2 into Profits," *Earth Institue*. [Online]. Available: https://blogs.ei.columbia.edu/2019/05/29/co2-utilization-profits/

[8] D. Sheldon, "Methanol Production - A Technical History," *Johnson Matthey Technology Review,* vol. 61, 3, pp. 172-182, 2017, doi: 10.1595/205651317X695622.

[9] D. J. Little, "Contruction and Demonstration of a Reactor System for Testing Methanol Synthesis Catalyst," Kansas State University, Manhattan, 1978.

[10] "Methanol Production - A Technical History," Johnson Matthey, Billingham, 2017.

[11] K. Kobl, Thomas, S.,Zimmermann, Y.,Parkhomenko,K.,Rober, A., "Power-law kinetics of methanol synthesis from carbon dioxide and hydrogen on copper-zinc oxide catalyst with alumina or zirconia supports," *Catalysis Today,* vol. 270, pp. 31-42, 2016.

[12] K. Xiao, Q. Wang, X. Qi, and L. Zhong, "For Better Industrial Cu/ZnO/Al2O3 Methanol Synthesis Catalyst: A Compositional Study," *Catalysis Letters,* vol. 147, pp. 1581-1591, 2017.

[13] S. Kuld *et al.*, "Quantifying the promotion of Cu catalysts by ZnO for methanol synthesis," *Science,* vol. 352, no. 6288, pp. 969-974, 2016, doi: 10.1126/science.aaf0718.

[14] T. Fujitani, M. Saito, Y. Kanai, T. Watanabe, J. Nakamura, and T. Uchijima, "Develpment of an active GA2O3 Supported Palladium Catalyst for the Synthesis of Methanol from Carbon Dioxide and Hydrogen," vol. 125, no. 2, pp. L199-L202, 1995.

[15] S. Collins, D. Chiavassa, A. Bonivardi, and M. Baltanas, "Hydrogen Spillover in Ga2O3-Pd/SiO2 Catalyst for Methanol Synthesis from CO2/H2," *Catalysis Letters,* vol. 103, pp. 1-2, 2005.

[16] Q. Tan, Z. Shi, and D. Wu, "CO2 Hydrogenation to Methanol over a Highly Active Cu-Ni/CeO2 Nanotube Catalyst," *Industrial & Engineering Chemistry Reserach,* vol. 57, no. 31, pp. 10148-10158, 2018, doi: 10.1021/acs.iecr.8b01246.

[17] H. Kong, H. Li, G. Lin, and H. Zhang, "Pd-Decorated CNT-Promoted Pd-Ga2O3 Catalyst for Hydrogenation of CO2 to Methanol," *Catalysis Letters,* vol. 141, pp. 886-894, 2011.

[18] J. D. Williams. "Carbon Nanotubes." (accessed.

[19] S. Zander, "Preparation and Characterization of Cu/ZnO Catalysts for Methanol Synthesis," Doctor of Philosophy, Institute of Chemistry, Technical University of Berlin, Berlin, 2012.

[20] B. Liang *et al.*, "Investigation on Deactivation of Cu/ZnO/Al2O3 Catalyst for CO2 Hydrogenation to Methanol," *Industrial & Engineering Chemistry Research,* vol. 58, pp. 9030-9037, 2019.
[21] R. Quinn, T. A. Dahl, and B. A. Toseland, "An evaluation of synthesis gas contaminants as methnaol synthesis catalyst poisons," *Applied Catalysis A: General,* vol. 272, pp. 61-68, 2004.
[22] M. Fichtl *et al.*, "Kinetics of deactivation on Cu/ZnO/Al2O3 methanol synthesis catalysts," *Applied Catalysis A: General,* vol. 502, pp. 262-270, 2015.
[23] M. Kurtz, H. Wilmer, T. Genger, O. Hinrichsen, and M. Muhler, "Deactivation of Supported Copper Catalysts for Methanol Synthesis," *Catalysis Letters,* vol. 86, pp. 77-80, 2003, doi: 10.1023/A:1022663125977.
[24] K. M. Vanden Bussche and G. F. Froment, "A Steady-State Kinetic Model for Methanol Synthesis and the Water Gas Shift Reaction on a Commercial Cu/ZnO/Al2O3 Catalyst," *Journal of Catalysis,* vol. 161, pp. 1-10, 1996, Art no. 0156.
[25] H. Bakemeier, P. R. Laurer, and W. Schroder, "Development and the Application of a Aathematical Model of the Methanol Synthesis," *Chem. Eng. Prog.,* vol. 66:98, 1970.
[26] K. Klier, "Methanol Synthesis," *Advances in Catalysis,* vol. 31, pp. 243-313, 1982, doi: 10.1016/S0360-0564(08)60455-1.
[27] P. Villa, P. Forzatti, G. Buzzi-Ferraris, G. Garone, and I. Pasquon, "Synthesis of Alcohols from Carbon Oxides and Hydrogen. 1. Kinetics of the Low-Pressure Methanol Synthesis," *Industrial & engineering chemistry process design and development,* vol. 24, no. 1, pp. 12-19, 1985, doi: 10.1021/i200028a003.
[28] G. H. Graaf, E. J. Stamhuis, and A. A. C. M. Beenackers, "Kinetics of Low-Pressure Methanol Synthesis," *Chemical Engineering Science,* vol. 43, no. 12, pp. 3185-3195, 1988.
[29] G. Leonzio, E. Zondervan, and P. U. Foscolo, "Methanol Production by CO2 Hydrogenation Analysis and Simulation of Reactor Performance," *International Journal of Hydrogen Energy,* vol. 44, pp. 7915-7933, 2019.
[30] C. A. Callaghan, "Kinectics and Catalysis of the Water-Gas-Shift Reaction: A Microkinetic and Graph Theoretic Approach," Worcester Polytechnic Institute, Worcester, 2006.
[31] G. H. Graaf, P. J. J. M. Sijtsema, E. J. Stamhuis, and G. E. H. Joosten, "Chemical Equilibria in Methanol Synthesis," *Chemical Engineering Science,* vol. 41, no. 11, pp. 2883-2890, 1985.
[32] PennState. "Peng-Robinson EOS (1976)." https://www.e-education.psu.edu/png520/m11_p2.html (accessed.
[33] S. H. Fogler, *Elements of Chemical Reaction Engineering*, 5 ed. Prentice Hall, 2016.
[34] S. Arab, J. M. Commenge, J. F. Portha, and L. Falk, "Methanol Synthesis from CO2 and H2 in multi-tubular fixed-bed reactor and multi-tubular reactor filled with monoliths.," *Chemical Engineering Research and Design,* vol. 92, no. 11, pp. 2598-2608, 2014.

MATLAB Code

Base Model Function File

```
function dFdW = Base(W,y,Dt,por,rhoc,Dp,mu,Tj,U)

%Initial Molar Flow
FA0 = y(1,1);%mol/s
FB0 = y(1,2);%mol/s
FC0 = y(1,3);%mol/s
FD0 = y(1,4);%mol/s
FE0 = y(1,5);%mol/s
FF0 = y(1,6);%mol/s
FT0 = FA0+FB0+FC0+FD0+FE0+FF0; %mol/s

%Initial Temp and Press
T0 = y(1,7);%K
P0 = y(1,8)*100000;%Pa

%Dynamic Molar Flow
FA = y(1); %mol/s
FB = y(2); %mol/s
FC = y(3); %mol/s
FD = y(4); %mol/s
FE = y(5); %mol/s
FF = y(6); %mol/s
FT = FA+FB+FC+FD+FE+FF; %mol/s

%Dynamic Temp and Press
T = y(7); %K
P = y(8); %bar

%Calculation of Reactor Properties
Ac = pi()*(Dt/2)^2; %m^2

%Calculation of Stream Properties
R = 8.314; %J/(mol*K)
molgasrho0 = P0/(R*T0); %mol/m^3
gasMW0 =
FA0/FT0*44.04+FB0/FT0*2.02+FC0/FT0*32.04+FD0/FT0*18.02+FE0/FT0*28.01+FF0/FT0*
16.04; %g/mol
rho0 = molgasrho0*gasMW0/1000; %kg/m^3
vflow0 = FT0/molgasrho0; %m^3/s
mflow0 = vflow0*rho0;
u = vflow0/Ac; %m/s

%Concentration Calculation
CA = FA/(FA+FB+FC+FD+FE+FF);
CB = FB/(FA+FB+FC+FD+FE+FF);
CC = FC/(FA+FB+FC+FD+FE+FF);
CD = FD/(FA+FB+FC+FD+FE+FF);
CE = FE/(FA+FB+FC+FD+FE+FF);
CF = FF/(FA+FB+FC+FD+FE+FF);
```

```
%Thermo Model Initiation
comp = [CA;CB;CC;CD;CE;CF];%Mole Frac
press = P*100000; %Pa
temp = T; %K
pressc = [7383000;1313000;8084000;22064000;3499000;4599000];%Pa
tempc = [304.21;33.19;512.5;647.096;132.92;190.564];%K
acentric = [0.223621;-0.215993;0.565831;0.344861;0.0481621;0.0115478];
BIP = [0.000    -0.162  0.023   0.120   0.000   0.0919
-0.162  0.000   0.000   0.000   0.092   0.016
0.023   0.000   0.000   -0.078  0.000   0.000
0.120   0.000   -0.078  0.000   0.000   0.000
0.000   0.092   0.000   0.000   0.000   0.030
0.092   0.016   0.000   0.000   0.030   0.000];
[fugcoef, zfactor] = fugacitycoef_multicomp_vapor(comp, press, temp, pressc,
tempc, acentric, BIP);

%Partial Pressure Calculation
PA = fugcoef(1,1)*FA/FT*P;%bar
PB = fugcoef(2,1)*FB/FT*P;%bar
PC = fugcoef(3,1)*FC/FT*P;%bar
PD = fugcoef(4,1)*FD/FT*P;%bar
PE = fugcoef(5,1)*FE/FT*P;%bar
PF = fugcoef(6,1)*FF/FT*P;%bar


%Kinetic Parameters
k1A = 0.499;
k1B = 17197;
k2A = 6.62E-11;
k2B = 124119;
k3A = 3453.38;
k3B = 1;
k4A = 1.07;
k4B = 36696;
k5A = 1.22E10;
k5B = -94765;

%Temp Corrected Kinetic Parameters
k1 = k1A*exp(k1B/(R*T));
k2 = k2A*exp(k2B/(R*T));
k3 = k3A*exp(k3B/(R*T));
k4 = k4A*exp(k4B/(R*T));
k5 = k5A*exp(k5B/(R*T));
k6 = 10^(3066/T-10.592);
k7 = 1/(10^(-2073/T+2.029));

%Rate Laws
r1 = k4*PA*PB*(1-
(1/k6)*(PD*PC/(PB^3*PA)))/(1+k3*(PD/PB)+k1*PB^(1/2)+k2*PD)^3; %mol/kg-cat/s
r2 = k5*PA*(1-k7*(PD*PE/(PA*PB)))/(1+k3*(PD/PB)+k1*PB^(1/2)+k2*PD); %mol/kg-
cat/s

%Heat Capacity Parameters (From DIPPR 2021)
CpAA = 24.99735;
CpAB = 55.18696;
CpAC = -33.69137;
```

```
CpAD = 7.948387;
CpAE = -0.136638;
CpBA = 33.066178;
CpBB = -11.36417;
CpBC = 11.432816;
CpBD = -2.772874;
CpBE = -0.158558;
CpCA = 59.70;
CpCB = 0;
CpCC = 0;
CpCD = 0;
CpCE = 0;
CpDA = 30.09200;
CpDB = 6.832514;
CpDC = 6.793435;
CpDD = -2.534480;
CpDE = 0.082139;
CpEA = 25.56759;
CpEB = 6.096130;
CpEC = 4.054656;
CpED = -2.671301;
CpEE = 0.131021;
CpFA = -0.703029;
CpFB = 108.4773;
CpFC = -42.52157;
CpFD = 5.862788;
CpFE = 0.678565;

%Heat Capacity Temperature Correction
CpA = CpAA+CpAB*T/1000+CpAC*(T/1000)^2+CpAD*(T/1000)^3+CpAE/((T/1000)^2);
%J/mol/K
CpB = CpBA+CpBB*T/1000+CpBC*(T/1000)^2+CpBD*(T/1000)^3+CpBE/((T/1000)^2);
%J/mol/K
CpC = CpCA+CpCB*T/1000+CpCC*(T/1000)^2+CpCD*(T/1000)^3+CpCE/((T/1000)^2);
%J/mol/K
CpD = CpDA+CpDB*T/1000+CpDC*(T/1000)^2+CpDD*(T/1000)^3+CpDE/((T/1000)^2);
%J/mol/K
CpE = CpEA+CpEB*T/1000+CpEC*(T/1000)^2+CpED*(T/1000)^3+CpEE/((T/1000)^2);
%J/mol/K
CpF = CpFA+CpFB*T/1000+CpFC*(T/1000)^2+CpFD*(T/1000)^3+CpFE/((T/1000)^2);
%J/mol/K

%Energy Balance
DelCp1 = CpC+CpD-3*CpB-CpA;%J/mol/K
DelCp2 = CpB+CpA-CpE-CpD;%J/mol/K
DelHrx1 = -49.5E3+DelCp1; %kj/mol-CO2
DelHRx2 = 41.2E3+DelCp2; %kj/mol-CO2
a = 4/(Dt*(1-por)*rhoc);
dTdW = (U*a*(Tj-T)-DelHrx1*r1-DelHRx2*r2)/...
    (FA*CpA+FB*CpB+FC*CpC+FD*CpD+FE*CpE+FF*CpF);

%Mole Balances
dFAdW = -r1-r2;
dFBdW = -3*r1-r2;
dFCdW = r1;
dFDdW = r1+r2;
```

```
dFEdW = r2;
dFFdW = 0;

%Pressure Drop (Ergan Equation)
G = rho0*u; %kg/m^2*s
B0 = G*(1-por)/(rho0*Dp*por^3)*(150*(1-por)*mu/Dp+1.75*G);
alpha = 2*B0/(Ac*rhoc*(1-por)*P0); %1/kg
dPdW = -alpha/(2*P*100000/(P0))*T/T0*FT/FT0;%Bar

dFdW = [dFAdW; dFBdW; dFCdW; dFDdW; dFEdW; dFFdW; dTdW; dPdW];
end
```

Base Model Driver Script File

```
options =[];

%Set Inlet Conditions (FA,FB,FC,FD,FE,FF,T,P)
y0 = [0.0002 0.0085 0 0 0.0003 0.0011 475 100];

%Set Span of Catalyst Weight
Wspan = [0 1];

%Set Reactor Properties
Dt = 0.08;

%Set Inlet Stream Properties
mu = 1.80E-05;

%Set Catalyst Properties
por = 0.4;
rhob = 1190;
rhoc = rhob/(1-por);
Dp = 0.0054;

%Set Heat Exchange Properties
Tj = 0;
U = 0;

%Run Base Model
[W,y]=ode23(@Base,Wspan,y0,options,Dt,por,rhoc,Dp,mu,Tj,U);

%Model Outputs
%Concentration Profile
CA = y(:,1).*100./(y(:,1)+y(:,2)+y(:,3)+y(:,4)+y(:,5)+y(:,6));
CB = y(:,2).*100./(y(:,1)+y(:,2)+y(:,3)+y(:,4)+y(:,5)+y(:,6));
CC = y(:,3).*100./(y(:,1)+y(:,2)+y(:,3)+y(:,4)+y(:,5)+y(:,6));
CD = y(:,4).*100./(y(:,1)+y(:,2)+y(:,3)+y(:,4)+y(:,5)+y(:,6));
CE = y(:,5).*100./(y(:,1)+y(:,2)+y(:,3)+y(:,4)+y(:,5)+y(:,6));
CF = y(:,6).*100./(y(:,1)+y(:,2)+y(:,3)+y(:,4)+y(:,5)+y(:,6));

%Conversion Profile
X_CO2 = (y(1,1)-y(:,1))./y(1,1);
GX_CO2 = 1-((y(:,1)+y(:,5))./(y(1,1)+y(1,5)));
Max_X_CO2 = max(X_CO2(:,1));
Max_GX_CO2 = max(GX_CO2(:,1));

%Selectivity
S_Methanol = y(:,3)./(y(1,5)+y(1,1));

%Normalized Catalyst Weight
Z = W./Wspan(1,2);

%Model Result Array
yfinal = [y(:,1) y(:,2) y(:,3) y(:,4) y(:,5) y(:,6) y(:,7) y(:,8) W(:,1)
Z(:,1) X_CO2(:,1) S_Methanol(:,1)];
```

Z-Factor Function

```
%% Z-factor calculation for Peng-Robinson EOS
% For PR-EOS, z-factor is calculated as the real roots of
% $Z^3 + (B-1)Z^2 + (A-2B-3B^2)Z - (AB-B^2-B^3) = 0$

function zfactor = calczfactor(a, b)

% Calculate the coefficients of cubic equation.
a1 = 1;
a2 = b - 1;
a3 = a - 2*b - 3*b^2;
a4 = -a*b + b^2 + b^3;

% Solve the cubic equation.
zroots = roots([a1 a2 a3 a4]);

% Choose the real roots.
zfactor = [];
for i = 1:3
    if imag( zroots(i) ) == 0
        z = real(zroots(i));
        zfactor = cat(1, zfactor, z);
    end
end

zfactor = sort(zfactor);
end
```

Mixing Rule Function 1

```
%% CALCULATE DIMENSIONLESS ATTRACTION AND COVOLUME, A & B

function [A, B] = calcab_multicomp(press, temp, pressc, tempc, acentric)

ncomp = size(pressc,1);
m = zeros(ncomp,1);
alpha = zeros(ncomp,1);
A = zeros(ncomp,1);
B = zeros(ncomp,1);
omegaa = 0.45724;
omegab = 0.0778;

for i = 1:ncomp

    % Calculate m.
    if acentric(i) > 0.49
        m(i) = 0.379642 + 1.48503*acentric(i) - 0.164423*acentric(i)^2 +
0.016666*acentric(i)^3;
    else
        m(i) = 0.37464 + 1.54226*acentric(i) - 0.26992*acentric(i)^2;
    end

    % Calculate reduced pressure and temperature.
    pressr = press/pressc(i);
    tempr = temp/tempc(i);

    % Calculate alpha.
    alpha(i) = ( 1 + m(i)*(1 - sqrt(tempr)) )^2;

    A(i) = omegaa*alpha(i)*pressr/tempr^2;
    B(i) = omegab*pressr/tempr;

end

end
```

Mixing Rule Function 2

```
% Calculate A and B for mixtures by using the classical mixing rule.

% $A_{mix} = \sum_[14] x_i x_j A_[14]$
% $A_[14] = \sqrt{A_i A_j}(1-k_[14])$
% $B_{mix} = \sum_{i}x_i B_i$
% $A_{mix2,j} = \sum_{i} A_[14] x_i$

% $k_[14]$ is binary interaction parameter.

function [Amix, Bmix, Amix2] = calcabmix(comp, A, B, BIP)

ncomp = size(comp,1);
% Calculate
Aij = zeros(ncomp, ncomp);
for i = 1:ncomp
    for j = 1:ncomp
        Aij(i,j) = sqrt(A(i)*A(j))*(1 - BIP(i,j));
    end
end

% Amix and Bmix are scalars.
Amix = comp'*Aij*comp;
Bmix = comp'*B;
% Amix2 is a vector.
Amix2 = Aij*comp;

end
```

Fugacity Coefficient Function 1

```
function fugcoef = calcfugcoef_multicomp(zfactor, A, B, Amix, Bmix, Amix2)

ncomp = size(A,1);
fugcoef = zeros(ncomp, 1);

c0 = 2*sqrt(2);
c1 = 1 + sqrt(2);
c2 = 1 - sqrt(2);

for i = 1:ncomp

    if zfactor < Bmix
        error('Z-factor must be larger than Bmix.\n');
    end

    fugcoef(i) = B(i)/Bmix*(zfactor - 1) - log(zfactor - Bmix) ...
        - Amix/(c0*Bmix) * (2*Amix2(i)/Amix - B(i)/Bmix) ...
        *log((zfactor + c1*Bmix)/(zfactor + c2*Bmix));

    fugcoef(i) = exp(fugcoef(i));

end

end
```

Fugacity Coefficient Function 2

```
% CALCULATE THE FUGACITY COEFFICIENT AND Z-FACTOR OF MULTI-COMPONENT SYSTEMS
% In this function, an appropriate z-factor is automatically chosen
% according to gibbs free energy if multiple roots are found.

function [fugcoef, zfactor] = fugacitycoef_multicomp(comp, press, temp,
pressc, tempc, acentric, BIP)

[A, B] = calcab_multicomp(press, temp, pressc, tempc, acentric);

[Amix, Bmix, Amix2] = calcabmix(comp, A, B, BIP);

zfactor = calczfactor(Amix, Bmix);

if (size(zfactor,1) > 1)
    zfactor = choosezfactor(zfactor, comp, A, B, Amix, Bmix, Amix2);
end

fugcoef = calcfugcoef_multicomp(zfactor, A, B, Amix, Bmix, Amix2);

end

%% SEARTCH AND RETURN AN APPROPRIATE Z-FACTOR
% Calculate dimensionless excess gibbs free energy, and return the z
% factor which minimizes the gibbs free energy.
function minzfactor = choosezfactor(zfactor, comp, A, B, Amix, Bmix, Amix2)

gibbsenergy = [];

for i = 1:size(zfactor,1)
    fugcoef = calcfugcoef_multicomp(zfactor(i), A, B, Amix, Bmix, Amix2);
    g = calcgibbsenergy(comp, fugcoef);
    gibbsenergy = cat(1,gibbsenergy,g);
end

[~, index] = sort(gibbsenergy);
minzfactor = zfactor(index(1));

end

function g = calcgibbsenergy(comp, fugcoef)

ncomp = size(comp,1);
g = 0;

for i = 1:ncomp
    if comp(i) ~= 0
        g = g + comp(i)*log(comp(i)*fugcoef(i));
    end
end

end
```

Fugacity Coefficient Function 3

```
% CALCULATE THE FUGACITY COEFFICIENT AND Z-FACTOR OF MULTI-COMPONENT SYSTEMS
% In this function, the maximum z-factor is automatically chosen.
function [fugcoef, zfactor] = fugacitycoef_multicomp_vapor(Comp, P, T, Cp,
Tc, Acentric, BIP)

[A, B] = calcab_multicomp(P, T, Cp, Tc, Acentric);

[Amix, Bmix, Amix2] = calcabmix(Comp, A, B, BIP);

zfactor = calczfactor(Amix, Bmix);

if (size(zfactor,1) > 1)
    zfactor = max(zfactor);
end

fugcoef = calcfugcoef_multicomp(zfactor, A, B, Amix, Bmix, Amix2);

end
```